Received: 5 July 2019 | Revised: 28 November 2019 | Accepted: 8 December 2019

DOI: 10.1002/jbm.b.34544

ORIGINAL RESEARCH REPORT

Society For Biomaterials | WILEY

Dual growth factor delivery using PLGA nanoparticles in silk fibroin/PEGDMA hydrogels for articular cartilage tissue engineering

Milad Fathi-Achachelouei[1] | Dilek Keskin[1,2,3] | Erhan Bat[1,4] | Nihal E. Vrana[5,6] | Aysen Tezcaner[1,2,3]

[1]Department of Biomedical Engineering, Middle East Technical University, Ankara, Turkey

[2]Center of Excellence in Biomaterials and Tissue Engineering (BIOMATEN), Middle East Technical University, Ankara, Turkey

[3]Department of Engineering Sciences, Middle East Technical University, Ankara, Turkey

[4]Department of Chemical Engineering, Middle East Technical University, Ankara, Turkey

[5]Inserm UMR 1121, Strasbourg, France

[6]SPARTHA Medical, Strasbourg, France

Correspondence
Nihal E. Vrana, SPARTHA Medical, 14B Rue de la Canardiere, 67100 Strasbourg, France.
Email: e.vrana@protipmedical.com or

Aysen Tezcaner, Department of Biomedical Engineering, Middle East Technical University, 06800 Ankara, Turkey.
Email: tezcaner@metu.edu.tr

Funding information
Horizon 2020 Framework Programme, Grant/Award Number: 760921; METU BAP, Grant/Award Number: GAP-310-2018-2847

Abstract

Degeneration of articular cartilage due to damages, diseases, or age-related factors can significantly decrease the mobility of the patients. Various tissue engineering approaches which take advantage of stem cells and growth factors in a three-dimensional constructs have been used for reconstructing articular tissue. Proliferative impact of basic fibroblast growth factor (bFGF) and chondrogenic differentiation effect of transforming growth factor-beta 1 (TGF-β1) over mesenchymal stem cells have previously been verified. In this study, silk fibroin (SF) and of poly(ethylene glycol) dimethacrylate (PEGDMA) were used to provide a versatile platform for preparing hydrogels with tunable mechanical, swelling and degradation properties through physical and chemical crosslinking as a microenvironment for chondrogenic differentiation in the presence of bFGF and TGF-β1 releasing nanoparticles (NPs) for the first time. Scaffolds with compressive moduli ranging from 95.70 ± 17.82 to 338.05 ± 38.24 kPa were obtained by changing both concentration PEGDMA and volume ratio of PEGDMA with 8% SF. Highest cell viability was observed in PEGDMA 10%-SF 8% (1:1) [PEG10-SF8(1:1)] hydrogel group. Release of bFGF and TGF-β1 within PEG10-SF8(1:1) hydrogels resulted in higher DNA and glycosaminoglycans amounts indicating synergistic effect of dual release over proliferation and chondrogenic differentiation of dental pulp stem cells in hydrogels, respectively. Our results suggested that simultaneous delivery of bFGF and TGF-β1 through utilization of PLGA NPs within PEG10-SF8(1:1) hydrogel provided a novel and versatile means for articular cartilage regeneration as they allow for dosage- and site-specific multiple growth factor delivery.

KEYWORDS
bFGF, cartilage tissue engineering, hydrogel, nanoparticles, TGF-β1

1 | INTRODUCTION

Articular cartilage tissue is a hyaline type cartilage tissue formed with the contribution of lateral plate mesenchymal cells during embryo development (Caplan, 1999). Being a part of connective tissue of diarthrodial joints, articular cartilage has been specialized to provide a smooth and lubricated surface with low frictional coefficient to minimize the stress on subchondral bone during the joint movement (Sophia Fox, Bedi, & Rodeo, 2009). Chondrocytes are metabolically active cells that reside in the dense extracellular matrix (ECM) of the

articular cartilage (Alford & Cole, 2005). ECM within cartilage is mostly composed of proteoglycans such as aggrecan, biglycan, fibromodulin decorin; collagens, especially Type II (90–95% of total collagen content); and minor elements such phospholipids, glycoproteins, lipids, and noncollagenous proteins (Barry, Boynton, Liu, & Murphy, 2001; Buckwalter & Mankin, 1998; Sophia Fox et al., 2009). Healing of articular cartilage is limited since there is low density of chondrocytes embedded in dense ECM resulting in restricted cell to cell interaction and it also lacks nerves, lymphatic vessels, and blood vessels (Buckwalter, 1998; James & Uhl, 2001). Direct trauma, indirect loading, or torsional loading can lead to damage to cartilage tissue (James & Uhl, 2001). Depending on its extent, cartilage damage can be irreversible such as in the case of osteoarthritis. Current treatments such as arthroplasty (Nikolaou, Chytas, & Babis, 2014), mosaicplasty (Hangody, Feczkó, Bartha, Bodó, & Kish, 2001), microfracture technique (Mithoefer et al., 2006), and cell transplantation (Brittberg et al., 1994) cannot fully reconstruct functional articular cartilage tissue.

To overcome surgical limitations, tissue engineering (TE) has been utilized for constructing articular cartilage tissue. As allogenic chondrocytes could evoke immune rejection and autologous chondrocytes are limited in number and require invasive isolation methods; utilizing other cell sources such as adult stem cells including adipose-derived stem cells (ADSCs; Wu et al., 2018), bone marrow-derived mesenchymal stem cells (BMMSCs; Ren et al., 2016), synovium-derived stem cells (SDSCs; Kubosch et al., 2018), and dental pulp stem cells (DPSCs; Mata et al., 2017) can provide necessary cell number in a less invasive manner for cartilage TE constructs. Simulating and mimicking natural tissue is an inevitable necessity for optimum maturation of stem cells for TE applications. Various factors can be utilized to modulate cellular maturation in signal transduction pathways, transcription factor expression, and protein regulation levels. Various factors including ECM component, mechanical and electrical signals, and soluble factors play can determine the fate of stem cells. Among soluble factors, growth factors (GF) as signaling proteins play a crucial role in orchestrating the cellular behavior, especially differentiation of stem cells. Various GFs that affect chondrogenic differentiation, homeostasis, and healing processes have been identified. Transforming growth factor-β (TGFs-β) family (Ying et al., 2018); bone morphogenetic proteins (BMPs) family (Chubinskaya & Rueger, 2017); insulin growth factor I (IGF-I; Zhang et al., 2017), fibroblast growth factor (FGF) family;(Khan, Muhammad, Scammahorn, Dell'Accio, & Vincent, 2018) platelet-derived growth factor (PDGF; Yokota et al., 2014) are among the most widely investigated GFs for articular tissue regeneration. Basic fibroblast growth factor (bFGF) can be found bound in the pericellular matrix, perlecan (Chia et al., 2009). Inhibitory effect of bFGF over interleukin-1 (IL-1) driven aggrecanolysis has been proven (Sawaji, Hynes, Vincent, & Saklatvala, 2008). There are studies showing the positive effect of bFGF on proliferation of BMMSCs and their synthesis of proteoglycans (Stewart, Byron, Pondenis, & Stewart, 2007). Transforming growth factor-beta 1 (TGF-β1), a 25 kDa polypeptide, can cause the activation and subsequent translocation of the TGF-β1 specific proteins, Smads, to the nucleus through binding to Type I and Type II membrane-bound heteromeric receptors. This event, in turn, regulates the gene expression specific for cartilage tissue through cell proliferation, cell differentiation and ECM metabolism (Grafe et al., 2018). In a recent study by Khan et al. (2018), the effect of bFGF on cartilage tissue repair has been investigated in bFGF knockdown mice. bFGF plays a role in MSC migration and adhesion to the damaged tissue and its absence was linked with diminished repair observed in knock-out mice studies. However, it has been suggested that a second signal, possibly mediated by released TGF-β is required for successful cartilage regeneration. Consequently, as it is known that bFGF has proliferative effect on MSCs (Stewart et al., 2007), it is possible to obtain higher cellular proliferation beside cellular migration and adhesion in the injured sites and upregulate the chondrogenesis effect through TGF-β1 (Park, Temenoff, Holland, Tabata, & Mikos, 2005).

GFs have short half-lives and can lose their biological activity due to their degradation or denaturation (Lee, Silva, & Mooney, 2011). Various delivery systems have been developed to extend half-life of GFs and control over the dosage and spatiotemporal release of GFs in ECM of the target tissue (Fathi-Achachelouei et al., 2019). One of the widely used delivery system of GFs is polymeric nanoparticles which can provide various rate of delivery due to their versatile and tailor-made properties (Alexis, Pridgen, Molnar, & Farokhzad, 2008; Petros & DeSimone, 2010; Vrana et al., 2014). Poly(lactic-co-glycolic) acid (PLGA) is a as widely used poly(ester) with well-established biodegradability and biocompatibility (Bobo, Robinson, Islam, Thurecht, & Corrie, 2016). For encapsulation of GFs, PLGA nanoparticles (NPs) can be prepared by various methods such as widely used double emulsion–solvent evaporation technique. This technique has widely been used for encapsulation of hydrophilic bioactive agents such as GFs and cytokines. However, denaturation or conformational change of agents during entrapment as a consequence of organic solvent used can decrease or totally eliminate their biological activity. Excipients are compounds which do not associate with therapeutic agents or polymeric matrix in such a way that change their chemical features, but they can increase the affinity between the bioactive agent and polymer, or change the distribution of the bioactive agent in the polymer matrix (Allison, 2008). In all cases, release profile will change due to various factors such as changes in diffusion rate, decrease in burst release, prolongation of the release period and protection of the bioactivity of sensitive therapeutics as a function of excipient and bioactive agent interaction. Different systems have been developed to examine the effect of versatile excipients such as poly(ethylene glycol) (PEG; Bock, Dargaville, & Woodruff, 2014), trehalose glycopolymer (Boehnke, Kammeyer, Damoiseaux, & Maynard, 2018), bovine serum albumin (BSA; Fröhlich et al., 2018), heparin (Li, Davidson, & Guelcher, 2009), and glucose(Li et al., 2009) on the release profile and bioactivity of the therapeutic agents. During the preparation of NPs, addition of other excipients such as heparin or Kolliphor P 188 can retain biological activity of GFs and control their release profile.

Hydrogels which are composed of highly hydrated natural or synthetic polymeric materials are one of the most suitable candidates to mimic the three-dimensional structure of the ECM. Depending on the

intrinsic nature of the polymers, various techniques such as physically (Kayabolen et al., 2017) or chemically crosslinking (Bertassoni et al., 2014; Bystroňová et al., 2018) methods can be utilized for the preparation of hydrogels. Silk fibroin (SF) as natural biopolymer has widely been used in TE applications due to its biocompatibility, and superior compressive modulus (Altman et al., 2003). Various techniques such as sonication (Wang, Kluge, Leisk, & Kaplan, 2008), vortexing (Kayabolen et al., 2017; Yucel, Cebe, & Kaplan, 2009), or electrical current (Leisk, Lo, Yucel, Lu, & Kaplan, 2010) can be applied to trigger the physical crosslinking of β-sheets in SF. PEG has been used in TE due to biocompatibility, ease of fabrication, and versatility of chemistry in monomer synthesis (Lin & Anseth, 2009; Moore & West, 2018). To prepare PEG hydrogels, it is possible to introduce crosslinking moieties such as acrylate or methacrylate to the chain end of PEG macromer and obtain photo-crosslinked PEG hydrogels such as poly(ethylene glycol) dimethacrylate (PEGDMA) under ultraviolet (UV) irradiation in the presence of a suitable photoinitiator such as Irgacure D-2959.

Various hydrogel systems containing GF loaded nanoparticles incorporated were reported in the literature for articular cartilage tissue regeneration (Ertan et al., 2013; Jung et al., 2009; Lim et al., 2010; Park, Yang, Woo, Chung, & Park, 2009). Generally, these systems concentrated more over-application of single type of GF such as TGF-β1 (Jung et al., 2009) or TGF-β3 (Park et al., 2009). Combination of different GFs contributes to maturation of stem cells and their chondrogenic differentiation. Therefore, studying the action of different GFs simultaneously in 3D hydrogel can improve and also mimic natural articular cartilage tissue regeneration at the same time. There a few studies focusing on hydrogel systems containing nanoparticles loaded with two different GFs [i.e., IGF-I/TGF-β1; Ertan et al., 2013) and BMP-7/TGF-β2 (Lim et al., 2010)] for articular cartilage TE. bFGF plays role in MSCs proliferation (Stewart et al., 2007), migration and adhesion of MSCs to the damaged articular cartilage tissue (Khan et al., 2018) and also, in articular cartilage repair through upregulation of multiple GFs in synovial fluid (Li et al., 2013); and TGF-β1 regulates cartilage tissue regeneration through cell proliferation, cell differentiation, and ECM metabolism (Grafe et al., 2018). Therefore, investigating the effect of controlled release of bFGF simultaneously with TGF-β1 in a hydrogel can provide a versatile tool for establishing a tissue-engineered construct that will mimic articular cartilage tissue.

The objective of this work was to develop SF-PEGDMA hydrogel system (a semi-degradable system for providing a stable scaffold for chondrogenesis) containing DPSCs and bFGF and TGF-β1 loaded PLGA NPs (for controlled dual delivery within the construct for improved proliferation and facilitated chondrogenic differentiation) that will provide a therapeutic means for the formation of a cartilage-like structure at the defect site. SF and PEGDMA were chosen as natural and synthetic polymers for hydrogels preparation through physically and photocrosslinking mechanism, respectively. Consequently, it was possible to provide more control over cellular responses including proliferation and differentiation by taking advantage of mechanical superiority of PEGDMA and cellular cues of fibroin along with their synergistic effect. Effect of PLGA NPs over mechanical properties of hydrogels was investigated. Effect of two different excipients on bioactivity and release profile of encapsulated GFs was studied. Additionally, effect of hydrogel composition on viability of DPSC by live/dead assay and chondrogenic differentiation by histology and immunohistochemical analysis was investigated.

2 | MATERIALS AND METHODS

2.1 | Materials

Poly(lactic-co-glycolic) acid (PLGA) 75:25, molecular weight (MW): 7–14 kDa from Boehringer Ingelheim (Germany) was used for particle production. Dichloromethane (DCM) from Merck (Germany) was used without further purification. Poly(vinyl alcohol) (PVA) Mowiol® 4-98 from Aldrich (Germany) was used as surfactant. Nevparin (heparin commercial trade name in Turkey) from Mustafa Nevzat İlaç Sanayi A. Ş. (Turkey) and Kolliphor P 188 from Sigma (Germany) were used as excipients in NPs production. SF from Akman İpek Company (Bursa, Turkey), and poly(ethylene glycol) (PEG) 4000 from Fluka were used for hydrogel preparation. Lithium bromide (LiBr) from Sigma-Aldrich (Germany) and sodium carbonate Na_2CO_3 from Sigma-Aldrich (Germany) were used for isolation of fibroin. Methacryloyl chloride from Alfa Aesar (Germany), triethylamine from Sigma-Aldrich (Germany) and diethyl ether from Sigma-Aldrich (Germany) were used for the synthesis of PEGDMA. 2-Hydroxy-4′-(2-hydroxyethoxy)-2-methylpropiophenone (Irgacure D-2959) from Aldrich (Germany) was used as the photoinitiator in hydrogel preparation. Sodium azide, (Sigma, Germany) and lysozyme from chicken egg white from Sigma (Germany) were used in the degradation studies. bFGF) from Peprotech and Transforming Growth Factor-β1 (TGF-β1) from Sigma (Germany) were used during preparation of GF loaded NPs. TGF-β1 enzyme-linked immunosorbent assay (ELISA) kit from Biomatik (Canada), and bFGF ELISA kit from Peprotech were used for quantitating the GFs. DPSCs were isolated using collagenase from Clostridium histolyticum, Type I A from Sigma (Germany) and dispase from Fluka were used. Cell culture studies were conducted using low glucose Dulbecco's Modified Eagle Medium (DMEM) from Biowest (France), fetal bovine serum (FBS) from Biowest (France), penicillin/streptomycin from Biowest (France), Trypan Blue solution from Sigma (Germany), trypsin/EDTA from Biowest (France), and dimethyl sulfoxide (DMSO) from Sigma-Aldrich (Germany). Cell viability studies performed using DMEM medium without phenol red from Bichrom (Germany), Alamar Blue from Invitrogen and live/dead Viability/Cytotoxicity kit from Invitrogen. Alcian Blue from Sigma (Germany) and paraformaldehyde from Sigma-Aldrich (Germany) were used for histology analysis. Papain from Papaya latex (Sigma, Germany), Chondroitin 6-sulfate sodium salt from shark cartilage (Sigma, Germany), 1,9-dimethylmethylene blue (DMMB; Aldrich, Germany), Ethylenediaminetetraacetic acid (EDTA; Sigma, Germany), cysteine hydrochloric acid (HCl; Fluka) were used for GAG quantification in hydrogels. Hoechst 33258 from Abcam (UK) was used for DNA quantitation. Immunohistochemical analysis was conducted using normal

goat serum (Abcam, UK), anti-collagen type II primary antibody (Abcam [ab34712], UK), goat anti-rabbit IgG H&L (Alexa Fluor® 488; Abcam [ab150077], UK), Triton X-100 (Sigma, Germany) and DRAQ5 (Cell Signaling Technology). All other chemicals were also of analytical grade and were used without further purification.

2.2 | Preparation of PLGA NPs

Empty PLGA NPs were prepared using double emulsion-solvent evaporation technique as described before with some modifications (Wang et al., 2015). Briefly, 100 mg of PLGA was dissolved in 3 ml of dichloromethane, then 200 μl of distilled water was added to the polymer solution. To form the first emulsion, mixture was probe sonicated (Branson SFX250) for 15 s at 250 W at 20 kHz, with 10% amplitude in the ice bath. Then, the emulsion was poured immediately into 20 ml of 5% PVA solution and probe sonicated with primary sonication condition for 55 s. Second emulsion was then poured into 70 ml 0.5% PVA solution while it was being stirred at 1,100 rpm at RT. To evaporate organic solvent, emulsion was stirred for 5 hr. Then, PLGA NPs were collected by centrifugation (Sigma 3-30k, Germany) at 19,000*g* for 25 min. NPs were washed twice with distilled water and after lyophilization for 48 hr, they were stored −80°C until use. bFGF and TGF-β1 loaded PLGA NPs were prepared with the same method by adding GFs to the inner aqueous phase with different excipients (Kolliphor P188 and heparin). Summary of the experimental conditions is provided in Table S1.

2.3 | Morphology, charge, and size distribution of PLGA NPs

After coating with gold/palladium using SC7640 Sputter Coater (Kent, UK), morphology of empty and bFGF loaded PLGA NPs was analyzed using scanning electron microscopy (SEM, FEI Nova Nano SEM 430). Size distribution of empty and bFGF loaded PLGA NPs was evaluated by two methods. First, Image J analysis software (NIH) was used to measure the diameters of 500 random PLGA NPs using SEM images. Second, size and charge of the empty and bFGF loaded PLGA NPs were determined through dispersing them in deionized water at a concentration of 200 μg/ml by dynamic light scattering (DLS) at 25°C with a Zetasizer Nano ZSP system (Malvern Instruments, Worcestershire, UK).

2.4 | Loading capacity, encapsulation efficiency and release profile, and kinetics of GFs

The amount of GFs entrapped in PLGA NPs was determined indirectly by determining the amount of unentrapped GFs in the supernatant and washes during NPs preparation by enzyme-linked immunosorbent assay (ELISA) kit. Standard calibration curve was constructed for each GF and encapsulation efficiency and loading capacity of NPs were calculated by the formula provided in the Supporting Information. Then, 10 mg of lyophilized PLGA NPs were dispersed into 2 ml of phosphate buffer saline (PBS, 0.01 M and pH 7.4) containing 0.02% sodium azide, and immersed into a shaking water bath at 37°C for 3 weeks. At specific time periods (6 hr, 1, 2, 3, 7, 11, 17, and 25 days), the whole medium was replaced with fresh medium after collecting PLGA NPs by centrifuging at 19,000*g* for 25 min. Discarded medium was frozen at −80°C for release analysis and amount of GFs released was determined by ELISA kit as described by the manufacturing protocol. To evaluate the release mechanism of the GFs from PLGA NPs prepared with different excipients, release data of experiments were fitted in zero-order (1), first-order (2), Higuchi (3), and Korsmeyer–Peppas (4) kinetic models using following formulas (Dash, Murthy, Nath, & Chowdhury, 2010).

$$Q_t = k_0 t \tag{1}$$

$$\log C_t = \log C_0 - \frac{k_1 t}{2.303} \tag{2}$$

$$Q_t = k_H \sqrt{t} \tag{3}$$

$$\frac{M_t}{M_\infty} = k_p t^n \tag{4}$$

Cumulative percent release versus time plot (zero-order), cumulative percent of GF remaining versus. time plot (first-order), cumulative percent release vs. square root of time plot (Higuchi) and log cumulative percent release versus log time plot (Korsmeyer–Peppas) plots were sketched to determine the best mechanism for release of bFGF and TGF-β1 and evaluate their kinetic models using rate constant (k), coefficient of determination (R^2), and n (for Korsmeyer–Peppas model) values.

2.5 | SF isolation and purification from silkworm cocoons

SF was isolated as described by Rockwood et al. with a small modification as described in Supporting Information (Rockwood et al., 2011).

2.6 | PEGDMA synthesis and characterization

PEGDMA was synthesized as described by Nuttelman, Tripodi, and Anseth (2004) with some modifications as described in Supporting Information. Proton nuclear magnetic resonance (^{1}H-NMR; Bruker AVANCE III 400 MHz) analysis was used to determine dimethacrylation degree of PEG.

2.7 | PEGDMA-SF hydrogel preparation

PEGDMA solution containing 0.05% (w/v% of total PEGDMA-SF solution) of 2-Hydroxy-4′-(2-hydroxyethoxy)-2-methylpropiophenone

(Irgacure D-2959) was prepared and sterilized using 0.2 μm filter. Then, 1.5 ml of 8% SF solution was poured into a 2 ml eppendorf and sonicated with probe sonicator (Branson SFX250) at a setting of 250 W, 20 kHz, 10% amplitude for 17 s at 10% amplitude. PEGDMA with different concentrations (10, 15, and 20%) and different volume ratios of SF:PEGDMA (3:1, 1:1, and 1:3) were added to the SF solution immediately after sonication and mixed by pipetting. The homogeneous solution was then added to a custom made Teflon mold and placed under a 365 nm UV lamp (VL-115, 1 × 15 W, Vilber Lourmat, France, 2,475 μW/cm^2 intensity at 10 cm distance from surface) at a distance of 10 cm distance and exposed to UV for 10 min for crosslinking. Crosslinked hydrogels were incubated for 30 min at 37°C. Afterward, hydrogels were punched with different biopsy punches for further experiments.

2.8 | Swelling and degradation of hydrogels

To evaluate swelling and degradation of hydrogels lyophilized samples with a dry weight of 70–75 mg were immersed into 5 ml of PBS solution (0.01 M, pH 7.4) containing 0.02% sodium azide and awaited in shaking water bath at 37°C for 4 weeks. Then, 10 μg/ml lysozyme was added to the PBS solution. At specific time points (0, 1, 7, 14, 21, 28 days), hydrogels were removed from PBS, their wet and dry weights were measured before and after lyophilization, respectively. At predefined time intervals (1, 4, 7, 14, 10, 14, 17, 21, 24, and 28 days) pH of PBS solution was measured and PBS was changed with fresh one.

2.9 | Mechanical tests of hydrogels

Unconfined compression test of wet hydrogels was performed to determine the mechanical properties of hydrogels. Hydrogel discs of 1 cm diameter and 5 mm height were obtained using 10 mm diameter biopsy punch and discs were placed in PBS until performing the experiments at room temperature (RT). Compression tests were done using 10 N load cell at a force rate of 1 mm/min up to 60% of the total height of hydrogels using mechanical testing device (Univert, CellScale, Canada). Compressive moduli and strength of the hydrogels were calculated from stress–strain curves.

To determine the effect of PLGA NPs on the compressive modulus and strength of the selected hydrogels, hydrogels containing PLGA NPs (5 and 10% of the total polymer weight) were prepared by adding NPs to the fibroin solution and homogenization with a probe sonicator for 17 s. Then, a given concentration and ratio of PEGDMA solution was mixed homogenously with fibroin solution. The final solution was added to the Teflon mold and UV irradiated for 10 min for crosslinking. Hydrogel discs with same dimensions were tested as described above.

2.10 | Chemical characterization of hydrogels

Fourier transform infrared spectroscopy (FTIR, Perkin Elmer Spectrum, Frontier, MA) analysis was performed for selected hydrogels to investigate the structural changes occurring upon hydrogel formation by photo-crosslinking. Hydrogel samples were lyophilized before analysis. PEGDMA powder was used as reference. The spectra were recorded from 400 to 4,000 cm^{-1} and at a resolution of 4 cm^{-1}.

2.11 | Morphology and pore size distribution of hydrogels

To observe microstructure of the hydrogels, they were lyophilized (5 mm diameter discs, 3 mm height), cut in horizontal and vertical axes; afterward, they were coated with gold and analyzed by SEM. Pore size distribution of hydrogels was measured using mercury porosimetry (Quantachrome Corporation, Poremaster 60) at low pressure (50 psi) after lyophilization of hydrogels. Contact angle of mercury was 140.00° and surface tension of mercury has been calculated as 480.00 erg/cm^2. For each experiment, 1 g of sample was used and mercury volume was normalized by the sample weight.

2.12 | Isolation of dental pulp stem cells

DPSCs were isolated from tooth of patients (18–25 years old) according to the procedure reported by Di Benedetto, Carbone, and Mori (2014) with some modifications as described in supplementary information. Ethical approval for use of tooth of patients was obtained from Middle East Technical University Human Researches Ethics Committee (IAEK) (No: 28620816/451).

2.13 | In vitro cytotoxicity test of PLGA NPs

To evaluate the cytotoxic effect of PLGA NPs over DPSCs 5 and 10 mg of empty PLGA NPs were incubated in 2 ml of low glucose medium (Dulbecco's Modified Eagle Medium (DMEM) with 10% fetal bovine serum (FBS), 100 U/ml penicillin, and 100 μg/ml streptomycin) for 11 days at 37°C. DPSCs at passage 5 were seeded in 24 well-plates at a seeding density of 1.0 × 10^4 cell/cm^2 and incubated in 600 μl of low glucose medium at 37°C. At specific time points (1, 4, 7, and 11 days) PLGA NPs were centrifuged and supernatant obtained was added over cells during media changes. Viability of DPSCs was measured using Alamar Blue assay at predetermined time points as described in Supporting Information.

2.14 | Effect of bFGF and TGF-β1 Released from PLGA NPs

To investigate the effect of bFGF and TGF-β1 released from 5 mg bFGF or TGF-β1 loaded PLGA NPs containing different excipients were incubated in 2 ml of low glucose medium and viability of cells was measured using Alamar Blue assay as described before.

2.15 | Viability of DPSCs in hydrogels

To determine viability of cells within the hydrogels, DPSCs were added to PEGDMA solution with a final concentration of 4.0×10^6/ml. PEGDMA solution was prepared using low glucose DMEM without phenol red. SF solution was probe sonicated for 17 s and added to PEGDMA solution containing cells and mixed with pipetting. Homogenous solution was added into Teflon mold and irradiated with UV light for 10 min. After formation of hydrogels, they were punched with 5 mm diameter biopsy punch and were placed in 48 well-plate containing 600 μl of low glucose medium. The gels were incubated in a carbon dioxide incubator at 37°C. The medium was changed every 3 days. At defined time points (1, 4, 7, and 14 days), viability of DPSCs in the hydrogels was evaluated using Alamar Blue assay.

2.16 | Viability of DPSCs entrapped in hydrogels containing PLGA NPs

Cell viability in hydrogels containing PLGA NPs was studied. PEGDMA10%:SF 8%-1:1 (PEG10-SF8(1:1)) was chosen as the hydrogel composition due to highest cell viability observed in this group (Figure 6a). bFGF loaded NPs with 0.5% heparin and TGF-β1 loaded NPs with 1.0% heparin as excipient were chosen because of the highest cell viability observed in these groups (Figure 5d,e, respectively).

Five different experimental groups were used: Empty hydrogel, hydrogel with 2.5 mg/ml empty NPs, hydrogel with 2.5 mg/ml bFGF NPs, hydrogel with 2.5 mg/ml TGF-β1 NPs, and hydrogel with 2.5 mg/ml bFGF NPs + 2.5 mg/ml TGF-β1 NPs; and named as control, empty, bFGF, TGF-β1 and bFGF + TGF-β1 group, respectively. After preparation of each group, hydrogels were punched with 5 mm diameter biopsy punch and incubated in 600 μl of low glucose medium at 37°C. Cell viability in the hydrogels was measured at predefined time intervals (1, 4, 7, 14, and 21 days) using Alamar Blue assay.

2.17 | Live/dead assay of DPSCs in hydrogels

Hydrogels prepared in the previous section were used to evaluate the effect of PLGA NPs and GF release on proliferation and morphology of cells. At specific time points (1, 7, 14, and 21 days), live/dead Viability/Cytotoxicity kit was used as instructed by manufacturer to observe live and dead DPSCs in hydrogels and images were captured using confocal laser scanning microscopy (CLSM; Leica DM2500, Germany). During taking of images in confocal microscope the brightness/contrast has been adjusted inevitably and minimally to prevent the background interface of SF, as it showed strong auto-fluorescence properties.

2.18 | Entrapped DPSCs quantification in hydrogels

Viability of DPSCs in hydrogels containing PLGA NPs at different time points (1, 7, 14, and 21 days) was determined to study cellular proliferation in hydrogels by digesting hydrogels in papain digestion solution to obtain cellular components. To each hydrogel (5 mm in diameter), 1 ml of papain digestion solution (1 mg/ml papain in 0.1 M phosphate buffer [PB] solution containing 5 mM L-Cysteine HCl and 5 mM Ethylenediaminetetraacetic acid, EDTA) was added. The hydrogels were incubated at 60°C for 16 hr and media were centrifuged at 15,000*g* for 20 min at RT. Then, 100 μl of supernatant was added to 900 μl of Tris-NaCl-EDTA (TNE) buffer and mixed with 1 ml of 200 ng/ml Hoechst 33258 dye. The solution was poured into 2 ml cuvette and fluorescence standard units (FSU) values were measured with spectroflourometer (Turner Biosystems Modulus Fluorometer 9200-000). The calibration curve was constructed using DNA contents of hydrogels in which different number of cells were encapsulated using the same protocol as described above. Increase in DNA amounts in hydrogel samples with time was interpreted as cell proliferation.

2.19 | Total sulfated glycosaminoglycan determination in hydrogels

Supernatant obtained after papain digestion of hydrogel samples was also used to determine GAG content of the hydrogels. GAG content was measured by 1,9-dimethylmethylene blue (DMMB) spectrophotometric assay by measuring absorbance at 525 nm. Chondroitin sulfate standards (0–15 μg/ml) were prepared in the supernatant from the empty hydrogel (without cell) to construct the calibration curve to determine GAG amounts produced by DPSCs. Total GAG content of hydrogels was normalized with DNA amount determined (μg/ng; Cui & Irudayaraj, 2015).

2.20 | Alcian blue staining for sulfated proteoglycans in hydrogels

To visualize the sulfated proteoglycans in hydrogels containing DPSCs and PLGA NPs, at specific time points (1, 7, 14, and 21 days) cells were fixed and hydrogels were sectioned as described in literature with some modifications (Ruan et al., 2013). Briefly, hydrogels were placed in PBS for 10 min and then fixed in 4% paraformaldehyde for 30 min. Afterward, 15 and 30% sucrose solutions in PBS were prepared. Solutions were added over hydrogels and incubated while shaking at RT each for 45 min in an increasing concentration order. Half of the medium of the hydrogels was then replaced with tissue freezing medium and hydrogels were shaken for 45 min. Afterward, hydrogels were placed in pure tissue freezing medium and frozen over methanol in dry ice. Frozen hydrogels were kept at −80°C freezer overnight. Sections of 15 μm thickness were taken from hydrogels by a cryomicrotome (Leica CM1510 S, Germany). The sections were placed over Superfrost™ Plus slides (ThermoFisher). Sections placed on the slides were deparaffinized by hydrating in PBS for 10 min and they were then incubated in Alcian Blue solution (1 g Alcian Blue in 100 ml 3% acetic acid solution, pH 2.5) at RT for 30 min (Crisan et al.,

2008). Slides were then washed twice in the tap water and then rinsed in the distilled water. Sections were counter stained with nuclear fast red solution (0.1 g nuclear fast red, Aluminium sulfate 5 g, distilled water 100 ml) and then washed in tap water for 1 min. Sections were then dehydrated by incubating in alcohol with increasing alcohol concentrations (from 70% to absolute one), each for 30 s. Finally, sections were cleared in xylene and mounted with solution made from nine parts of glycerol and 1 part PBS for preserving sections and imaging using phase contrast microscope (Nikon, Eclipse TS 100, Japan).

2.21 | Immunohistochemical analysis

To visualize collagen type II deposition by the cells, cells in hydrogels were fixed with 4% paraformaldehyde for 15 min at predefined time intervals (1, 7, 14, and 21 days) and kept at 4°C until analysis. Fixed hydrogels were deparaffinised by hydrating in PBS three times, each for 5 min. Then, hydrogels were immersed in PBS containing 0.1% Triton X-100 for 15 min to permeabilize cell membrane. After washing hydrogels three times with PBS, hydrogels were immersed in goat serum (1:10 diluted in PBS) for 1 hr at RT to block nonspecific antibody binding. Anti-collagen type II primary antibody was diluted 1:200 in PBS containing 0.1% BSA and incubated overnight at 4°C. After washing with PBS, hydrogels were then incubated with goat anti-rabbit IgG H&L secondary antibody (diluted 1:400 in PBS) for 1 hr at RT. After washing with PBS, nuclei of cells were stained by DRAQ5 for 10 min in RT and washed three times with PBS. Hydrogel sections were examined with confocal laser scanning microscopy (CLSM; Leica DM2500, Germany) for collagen type II analysis. During taking of images in confocal microscope the brightness/contrast has been adjusted inevitably and minimally to prevent the background interface of SF, as it showed strong auto-fluorescence properties.

2.22 | Statistical analysis

All tests conducted were performed at least in triplicates, otherwise it is indicated. For comparing groups for significant differences, one-way analysis of variance (ANOVA) with Tukey's Comparison Test (SPSS-22 Software, SPPS Inc.) was used. Pairwise comparisons were performed at a level of significance of 0.05.

3 | RESULTS

3.1 | PLGA NPs morphology, charge, and size characterization

Morphology of empty PLGA NPs prepared by double emulsion–solvent evaporation technique was evaluated using SEM images (Figure 1a). NPs had round, spherical shape with a submicron size distribution. To determine the charge on the surface of PLGA NPs zeta potential analysis was performed. DLS analysis of at 25°C showed that PLGA NPs had an average zeta potential value of −27.10 ± 8.40 mV (Figure 1b). Size of NPs was determined using both SEM images (Figure 1c) and zeta size analysis (Figure 1d). From SEM images diameter of 500 NPs was measured. Particle diameter ranged between 87.54 and 917.93 nm with an average of 246.07 ± 119.29 nm. Diameter size distribution of NPs revealed that 91% of the particles had a diameter less than 400 nm. Zeta size analysis showed similar average particle size (274.34 ± 42.56 nm; Figure 1d). Both analyses revealed that particles produced were nanosized and had a submicron size distribution. SEM images and particle size distribution of bFGF loaded PLGA NPs were analyzed to understand the NPs size variation after loading the GF. Similar to the empty PLGA NPs, bFGF loaded NPs have shown similar characteristics with spherical shape and a submicron size distribution (Figure S1a). bFGF loaded NPs showed zeta potential value of −28.40 ± 5.85 mV (Figure S1b). Particle diameter measurement of bFGF loaded NPs from SEM images revealed that particle had a particle size in the range of 75.3 and 1,145.5 nm with average diameter of 253.13 ± 134.43 nm. Particles with less than 400 nm included 90% of the whole particles population (Figure S1c). Zeta size analysis revealed similar size of NPs (267.24 ± 70.24 nm; Figure S1d).

3.2 | Loading capacity, encapsulation efficiency and release profile of GFs

To study the effect of different excipients on in vitro release profile of bFGF and TGF-β1 from NPs, two sets of experiments were conducted (n = 3 for each group and experiment). In the first set of experiments, Kolliphor P 188 and heparin with different concentrations were utilized as excipients (Table S1, Experiments 1–4). When Kolliphor P 188 was used as excipient, NPs had encapsulation efficiency (EE) of 94.70 ± 0.21%. EE of NPs prepared with heparin excipient showed a concentration dependency. As concentration of heparin was decreased from 1.0 to 0.1%, EE of NPs increased from 80.12 ± 0.41% to 91.72 ± 0.20%. Loading capacity (weight of protein (μg)/weight of polymer (mg)) in heparin bearing groups increased from 8.11 ± 0.21% to 9.04 ± 0.22% as the concentration of heparin was decreased (Table S2). Release profile study showed that at the end of the first day a minimum of 135.34 ± 4.21 ng and a maximum of 356.60 ± 4.54 ng releases were observed for 0.1% Kolliphor P 188 and 0.5% heparin groups, respectively (Figure 2a). The release profile showed a burst release at the end of first day and low bFGF release until the 17th day for all groups. At the end of 25 days of release study, a minimum of 18.32% and a maximum of 51.39% cumulative release percentages were released from 0.1% Kolliphor P 188 and 0.5% heparin groups, respectively (Figure 2b). Considering different concentrations of heparin, interestingly NPs prepared with 0.5% heparin showed higher cumulative release (51.39%) than prepared with 1.0%

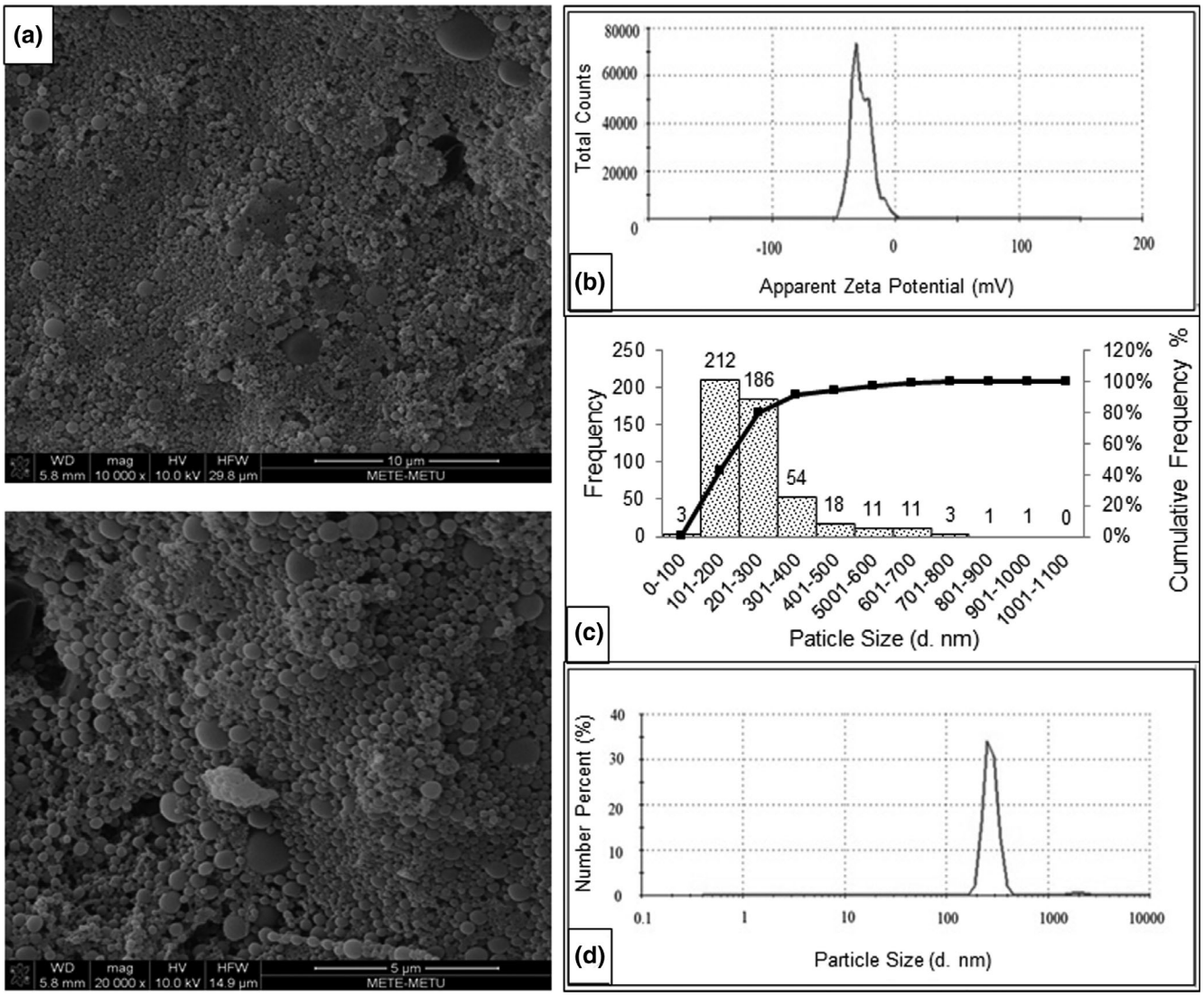

FIGURE 1 SEM images of PLGA NPs (scale bar; top: 10 µm, bottom: 5 µm) (a), zeta potential analysis result of empty PLGA NPs (b), particle size distribution of empty PLGA NPs constructed with diameter measurements from SEM images (c), and obtained with zeta sizer (d)

heparin (33.02%), while cumulative release was lower for NPs prepared with 0.1% heparin (22.03%). Similarly, heparin and Kolliphor P 188 were utilized as excipients for the TGF-β1 NPs experiments (Table S1, Experiments 5–8). EE for all Kolliphor P 188 and heparin bearing NPs groups was over 98.50 ± 0.21% (Table S3). Slowest release was observed for Kolliphor P 188 and 0.1% heparin bearing NPs groups with 2.20 and 1.60% release, respectively (Figure 2b). No change in released amounts was observed after 2 days for these two groups which could be an indication of the TGF-β1 denaturation during the encapsulation procedure. For 0.5 and 1.0% heparin groups, 11.96 and 13.28% cumulative release were observed, respectively, which indicates that there was a heparin concentration dependent release of TGF-β1 from PLGA NPs. The amounts of TGF-β1 released for heparin 1.0% and 0.5% were 75.21 ± 2.10 ng and 80.11 ± 2.94 ng at the end of first day and it increased to 110.21 ± 0.12 ng and 99.32 ± 0.10 ng, respectively, at the end of third day (Figure 2a).

3.3 | Kinetics of GF release

In vitro release data of all experimental groups (Table S1) were fitted to zero order, first order, Higuchi and Korsmeyer–Peppas models, and rate constants (K_0, K_1, K_H, and K_P), n value and coefficients of determination (R^2) were calculated. The best predicting kinetic behavior model for both bFGF (Table S4) and TGF-β1 (Table S5) based on the R^2 values was Korsmeyer–Peppas model. This model is based on the power law, and it describes the drug release through semi-empirical equation $\frac{M_t}{M_\infty} = k_p t^n$ from a polymeric system. Here, value of n as release exponent provides the releasing mechanism which is geometry dependent. A value of 0.43 or below for sphere suggests Fickian diffusion controlled release, for $0.43 < n < 0.85$ anomalous diffusion, and for $n > 0.85$, case II diffusion), it is possible to predict the release mechanism (Mehta et al., 2017). As the n value of Korsmeyer–Peppas model for all groups was <0.43, it was concluded that release observed for all groups followed Fickian or quasi-Fickian diffusion (Siepmann & Siepmann, 2008).

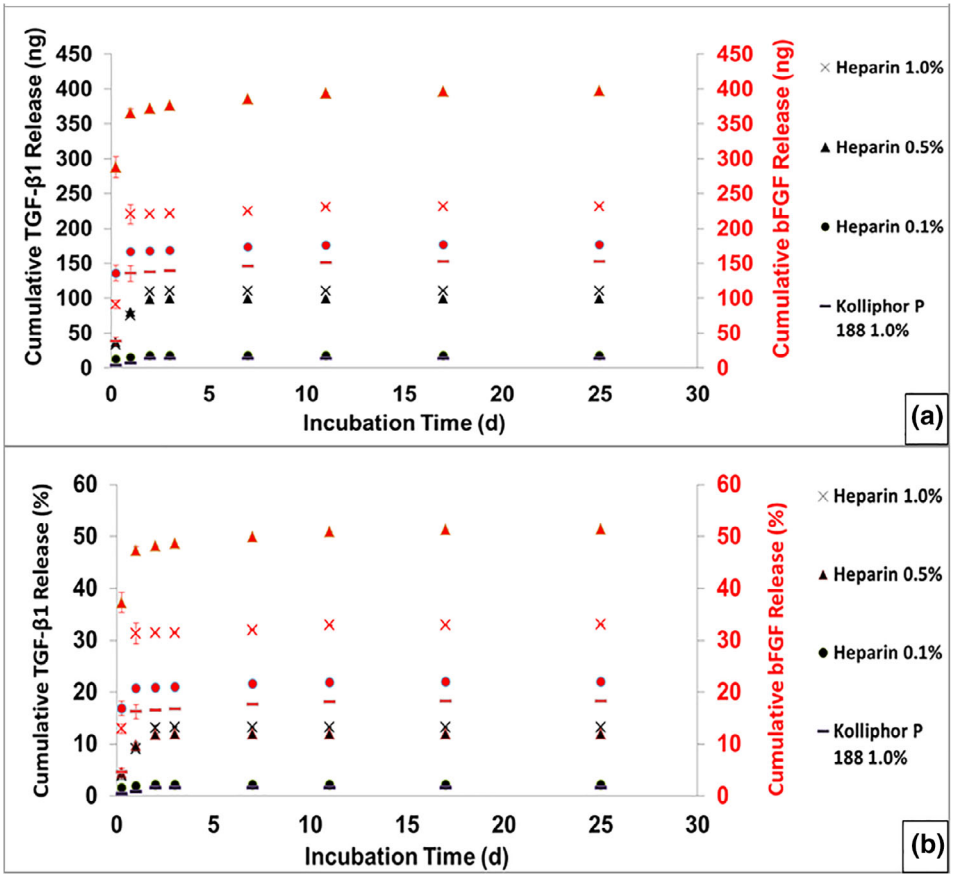

FIGURE 2 Cumulative amounts released of bFGF (red) and TGF-β1 (black) (a) and cumulative release percentages of bFGF (red) and TGF-β1 (black) (b) from PLGA NPs with heparin and Kolliphor P 188 excipients

3.4 | SF and PEGDMA preparation

After isolation of SF, autoclaving was performed for sterilization. Autoclaving can affect protein integrity through shortening of the polymer chain, sonication time, and consequently gelation time of SF should be optimized prior to each experiment (Rockwood et al., 2011). Dimethacrylation of PEG was done through reaction of hydroxyl group of the PEG with methacryloyl chloride in the presence of triethylamine as a mild base (Figure S2a). Degree of methacrylation of PEGDMA was determined using 1H-NMR analysis (Figure S2b). To do so, ratio of integral value for ethylene protons in the repeating unit of PEGDMA (a) to the protons at the vinyl group (b) was calculated as 2.95 which corresponded to a degree of methacrylation of 73.7%.

3.5 | Compressive modulus and strength of hydrogels and effect of PLGA NPs on mechanical properties

Hydrogels with 1 cm diameter and 5 mm height were tested with unconfined compression test using 10 N load at 60% of their total height (n = 4 for each experiment). Compressive moduli of pure PEGDMA hydrogels decreased from 337.38 ± 19.30 to 57.08 ± 14.94 kPa as the polymer concentration was lowered from 20% to 10%, respectively (Figure 3a). It was reported that 10, 15, and 20% PEGDMA hydrogels prepared with PEGDMA with weight average molecular weight (M_w) of 4,600 Da had equilibrium moduli of 50, 190, and 270 kPa when tested under unconfined compression.(Nguyen, Hwang, Chen, Varghese, & Sah, 2012; Roberts, Earnshaw, Ferguson, & Bryant, 2011) Difference of our results for 15 and 20% PEGDMA groups from literature could be due to difference in degree of crosslinking and MW of PEG monomer which could change the crosslinking density and consequently mechanical properties of hydrogels. In pure fibroin groups, compressive moduli decreased from 353.45 ± 31.20 to 161.53 ± 39.43 kPa as the concentration was halved. Obtained modulus value for SF 4% (SF4) group (161.53 ± 39.43 kPa) was in accordance with those reported in literature, but for the compressive modulus reported for SF 8% (SF8) group in literature was higher than our result (353.45 ± 31.20 kPa) which could be due to autoclaving we conducted (Kim et al., 2004). For blend hydrogel groups, increasing the concentration of PEGDMA from 10% to 20% resulted in an increase in compressive moduli for all SF to PEGDMA ratios. Compressive strength of pure PEGDMA groups significantly decreased (from 12.01 ± 1.31 to 2.04 ± 0.24 MPa) as the PEGDMA concentration was halved (Figure 3b). As the concentration of pure fibroin was halved, significant decrease in compressive strength (21.86 ± 2.16 to 2.16 ± 0.33 MPa) was observed.

Incorporation of delivery systems such as PLGA NPs can change the mechanical properties of hydrogels. To provide homogeneous distribution of NPs within the hydrogels, PLGA NPs were added to the SF solution and sonicated together. Therefore, hydrogels in which highest cellular viability (Figure 6a) was observed was selected for

incorporation of PLGA NPs (5 and 10% of total dry weight of polymers; $n = 4$ for each experiment). Incorporation of 10% PLGA NPs into 10 and 15% pure PEGDMA (PEG10 and PEG15, respectively) increased the compressive modulus from 55.47 ± 12.91 and 134.50 ± 11.61 kPa to 197.33 ± 19.85 and 197.10 ± 28.92 kPa, respectively (Figure 3c). For the SF8 group encapsulation of PLGA NPs decreased the compressive modulus of hydrogels from 344.87 ± 13.50% to 260.50 ± 1.77% kPa. In blend hydrogels with the exception of PEG10-SF8(1:1), addition of 10% PLGA NPs significantly increased the compressive modulus. Addition of 10% PLGA NPs in both PEG15

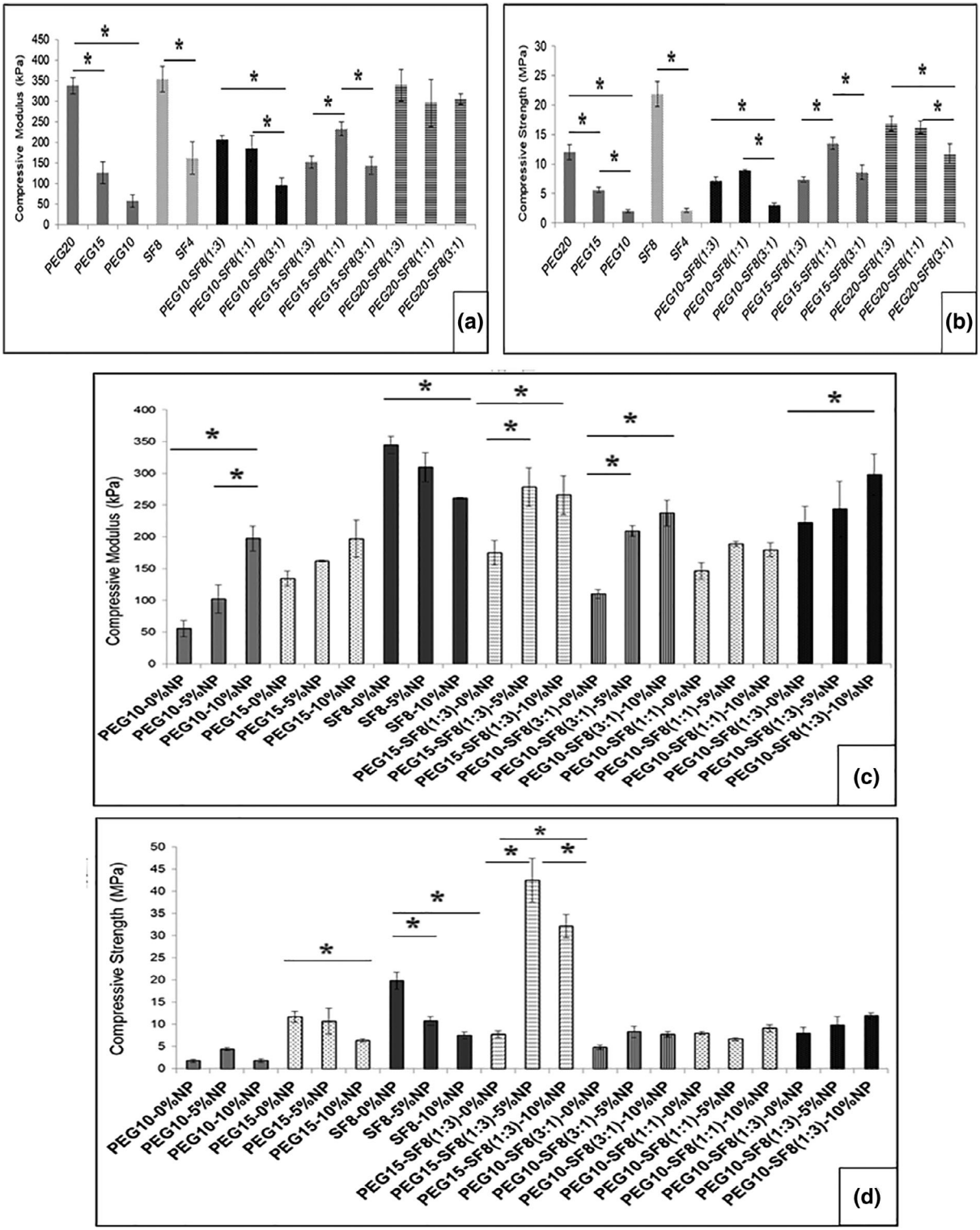

FIGURE 3 Compressive moduli (a) and strength (b) of hydrogels ($n = 4$), Effect of PLGA NPs on the compressive modulus (c) and strength (d) of hydrogels ($n = 4$). *Statistically significant differences between members of each group ($p \leq .05$)

and SF8 groups decreased their compressive strength from 11.68 ± 1.23 and 19.84 ± 1.89 MPa to 6.38 ± 0.40 and 7.51 ± 0.78 MPa, respectively (Figure 3d). For blend PEG10-SF8 hydrogels (in all ratios) addition of PLGA NPs did not significantly change the compressive strength, but for the PEG15-SF8 (1:3) group significant increase in the compressive strength of the hydrogels was observed.

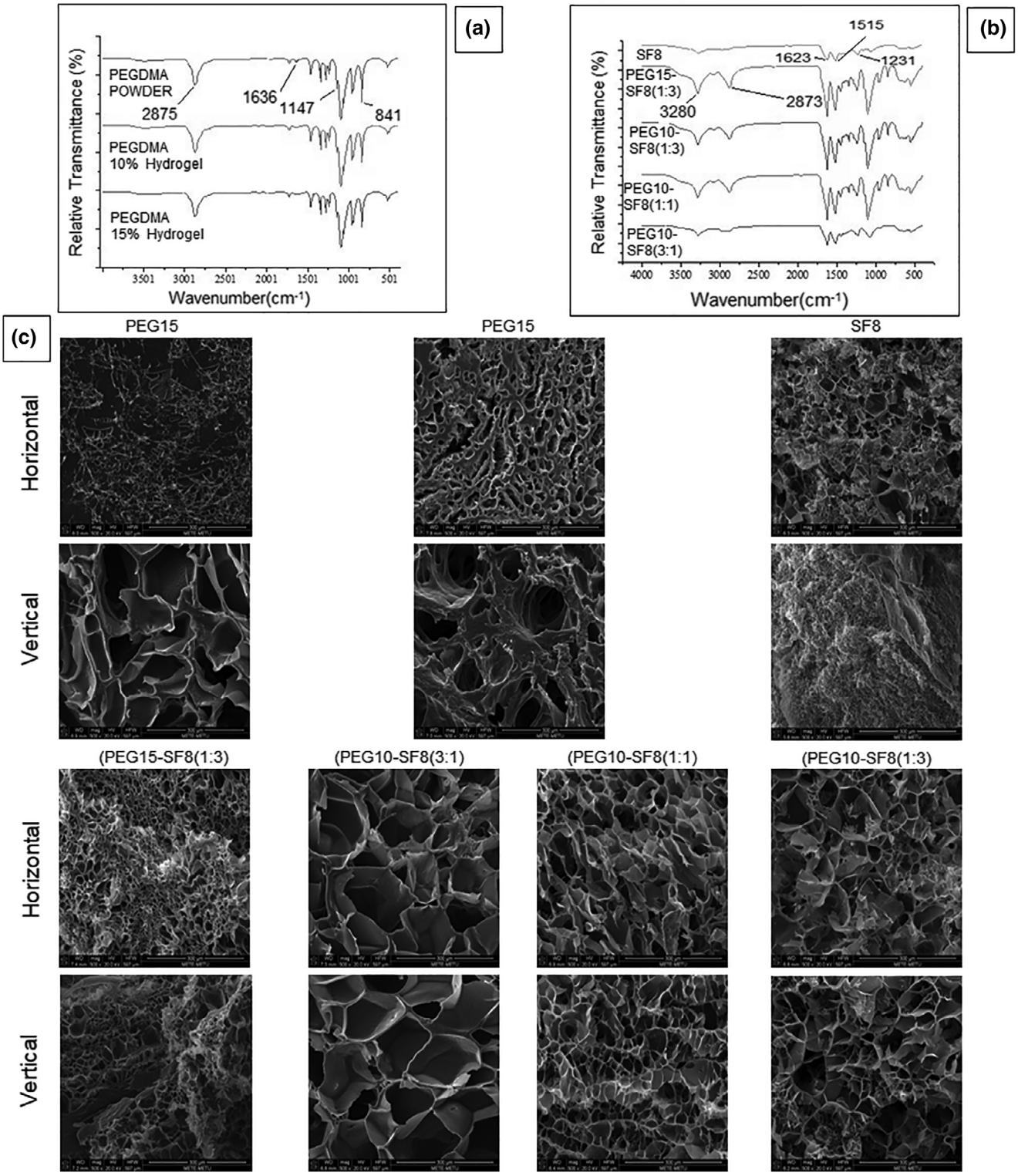

FIGURE 4 FTIR spectra of PEGDMA of different concentrations before and after gelation (a) and pure silk fibroin hydrogels and its blend hydrogels with PEGDMA (b), SEM images of horizontal and vertical cross sections of hydrogels (c) (scale bar = 300 μm)

3.6 | Swelling, degradation, and pH change of hydrogels

Swelling ratio (Figure S3) and degradation (Figure S4) of hydrogels were evaluated through immersing the hydrogels into PBS at 37°C (n = 3). For pure PEGDMA and pure fibroin groups, decreasing hydrogel concentration increased the swelling ratio. In the blend hydrogels as the ratio of fibroin to PEGDMA was increased from 1:3 to 3:1, swelling ratio decreased. For pure PEGDMA groups, less than 20% weight loss was observed at the end of 28 days. At the end of 2 weeks of incubation SF4 group had the highest weight loss (97.93 ± 2.12% loss of their initial weights) whereas SF8 group lost 73.81 ± 8.28% of their initial weights at the end of 28 days. In blend hydrogels, lower PEGDMA concentration led to a higher degradation rate. At the end of 28 days, 20% PEGDMA containing groups had a cumulative weight loss of 28.50 ± 6.42% (PEG20-SF8-(1:3)), while PEG10-SF8-(1:3) and PEG15-SF8(1:3) groups had lost 89.93 ± 7.95 and 80.567 ± 9.25% of their initial weights, respectively. Enzymatic degradation of hydrogels was studied in 10 μg/ml lysozyme enzyme solution in PBS (Figure S5). No significant difference in weight loss results was observed in PBS and enzyme solution. pH of PBS (Table S6) and lysozyme solution (Table S7) was also measured for 28 days at specific time points.

3.7 | Chemical characterization of hydrogels

FTIR analysis was performed for the selected hydrogels to investigate the structural changes occurring upon hydrogel formation by photocrosslinking. PEGDMA powder was used as reference and compared to 10 and 15% PEGDMA hydrogels in Figure 4a. Peak at 2,875 cm^{-1} is a characteristic peak PEGDMA which is assigned to

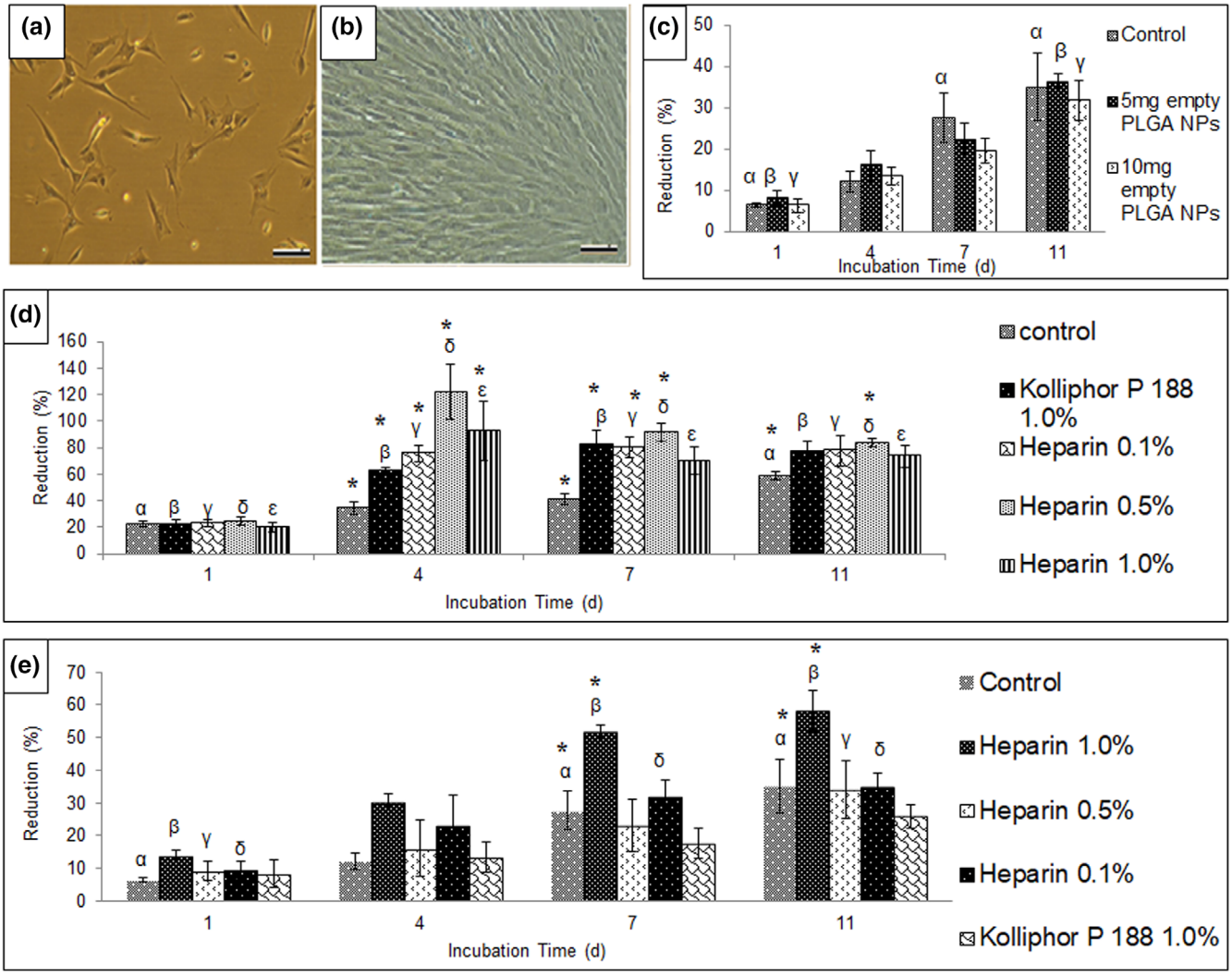

FIGURE 5 Phase contrast images of human DPSCs on first day after isolation (a), cells (sixth passage) at confluency (b). Scale bar is 100 μm. Effect of different amounts of PLGA NPs on viability of DPSCs (c), effect of bFGF (d), and TGF-β1 (e) released from PLGA NPs prepared with different excipients on viability of DPSCs. α, β, γ, δ, and ε show significant difference of results of day one and other incubation days ($p \leq .05$). * Statistically significant differences between control group and experimental groups at the same day ($p \leq .05$)

symmetric methylene stretching and it is not involved in photopolymerization (Hwang, Noh, Kim, & Jung, 2015). Three peaks at 841, 1147 and 1,636 cm^{-1} are characteristic peaks for the dimethacrylate groups (C–H, C=C and C–O) which significantly decreased after photopolymerization and hydrogel formation (Killion, Geever, Devine, Kennedy, & Higginbotham, 2011). FTIR spectra of SF8 hydrogel group and blend hydrogels were evaluated for determining success of hydrogel preparation (Figure 4b). Three characteristic peaks at 1,231, 1,515, and 1,623 cm^{-1} which belong to the amide I (CO stretching), amide II (NH deformation and CN stretching) and amide III (CN stretching and NH deformation) were observed in the pure fibroin spectrum (Zaharia et al., 2012). Characteristic broad peaks of fibroin for OH and NH groups at 3,280 cm^{-1} and PEGDMA peak at 2,873 cm^{-1} were used as reference in the blend hydrogels, as both peaks will not change after gelation. For PEG15-SF8(1:3) and PEG10-SF8(1:3) same intensity was observed but as the PEGDMA portion in blend hydrogels increased, intensity of the characteristic peak at 3,280 cm^{-1} for SF decreased and peak

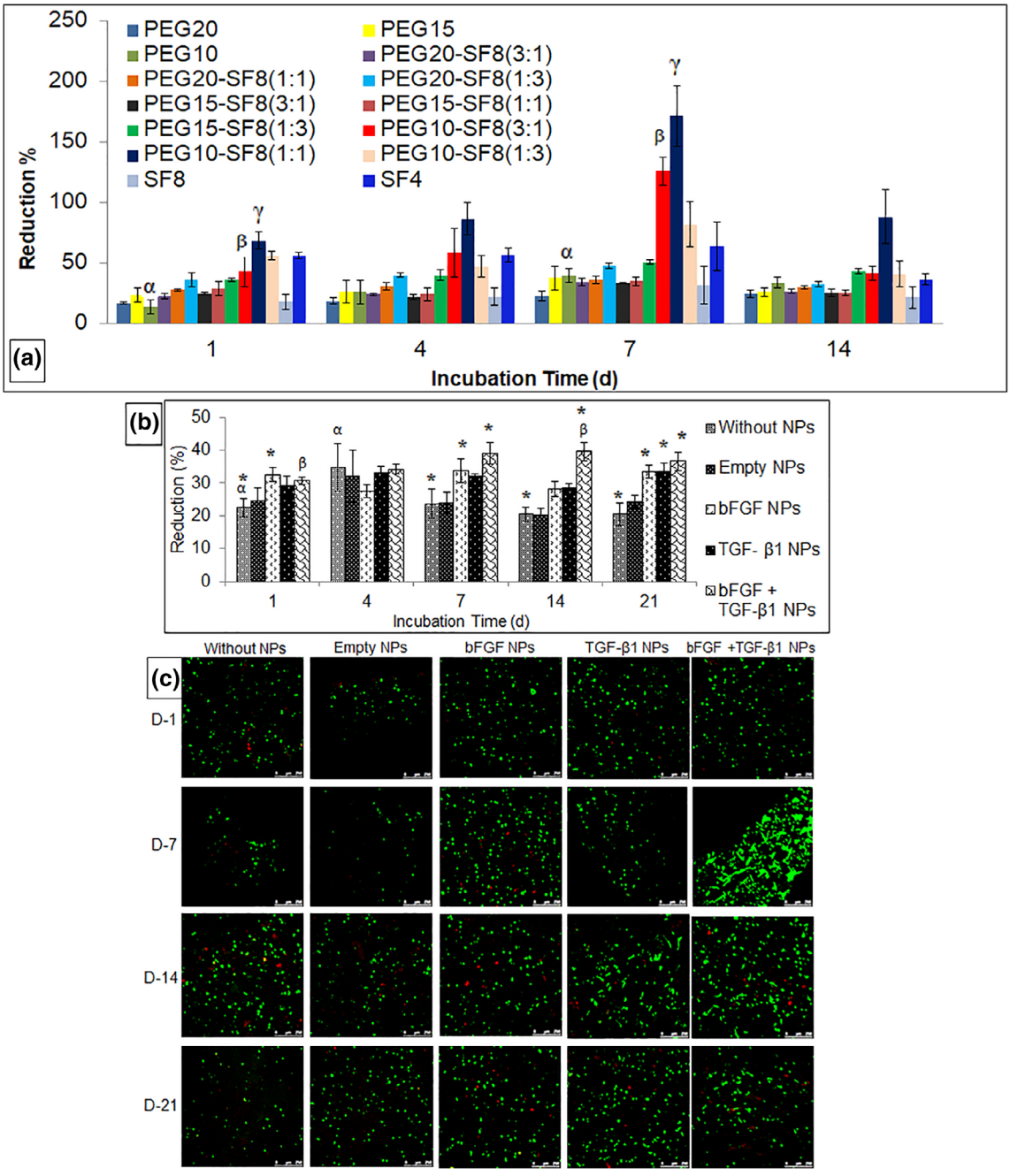

FIGURE 6 Viability of DPSCs entrapped in hydrogels (a), viability (b), and live/dead assay (c) of DPSCs entrapped in PEG10-SF8 (1:1) hydrogel. Green stained (calcein-AM) cells are live cells, red stained (ethidium homodimer-1) cells are dead cells (10× magnification, scale bar = 250 μm). α, β, and γ show significant difference at a significance level of 0.05). *Statistically significant differences between without NPs group and experimental groups at the same day ($p \leq .05$)

intensity at 2,873 cm^{-1} which was the characteristic peak for PEGDMA increased.

3.8 | Morphology and pore size distribution of hydrogels

SEM analysis was performed on vertical and horizontal cross sections of the selected hydrogels obtained after lyophilization (Figure 4c). For 15 and 10% pure PEGDMA larger pore size was observed in the vertical cross section compared to pore size in the horizontal cross section. SF8 group had the smallest pore size compared to other hydrogel groups both in horizontal and vertical cross sections, which was an indication of highly interconnected pore structure within the fibroin hydrogel. In the blend groups, PEG15-SF8(1:3) group had smaller porosity in both horizontal and vertical cross-section images compared to 10% PEGDMA groups. For blend hydrogels (PEG10-SF8(3:1), (1:1), and (1:3)), the pore size decreased in both horizontal and vertical cross section images as the ratio of the fibroin was increased from 1:3 to 3:1.

To evaluate the pore size distribution mercury porosimetry (n = 3) analysis at low pressure (50 psi) of the lyophilized hydrogels was utilized (Ji, Khademhosseini, & Dehghani, 2011; Kuberka, Von Heimburg, Schoof, Heschel, & Rau, 2002; O'Brien et al., 2007). For 15% (Figure S6a) and 10% (Figure S6b) pure PEGDMA pore size distribution showed a shift toward larger pore sizes as the concentration was lowered which was in accordance with SEM images. Similar pore size distribution was observed for SF8 (Figure S6c) and blend hydrogel PEG15-SF8(1:3) group (Figure S6d). Hydrogel groups with higher fibroin content had larger pore size (Figure S6f) and narrow pore size distribution. However, PEG10-SF8(1:3) (Figure S6g) had broader pore size distribution that ranged from 4 to 200 μm. Pore size distribution in PEG10-SF8(3:1) and (1:1) groups ranged from 40 to 400 μm.

3.9 | Isolation of DPSCs

DPSCs show high plasticity, accessibility and multipotent differentiation capacity, therefore they can be used as reliable stem source for TE applications (Huang, Gronthos, & Shi, 2009). After isolation of DPSCs, cell expansion was done by sub-culturing up to sixth passage. Morphology of isolated cells takes different forms as endothelial-like, spindle-like and or epithelial-like (Figure 5a); but after subculturing (passage 6) cells gain fibroblastic, spindle-like morphology (Figure 5b; Akmal et al., 2014; Huang et al., 2009).

3.10 | In vitro cytotoxicity test of PLGA NPs

Elution test using extracts of PLGA NPs was performed to evaluate the cytotoxicity of NPs on DPSCs. Then, 5 and 10 mg of empty PLGA NPs were incubated in low glucose medium at 37°C and at specific time points the medium was centrifuged and supernatant obtained was added to DPSCs. For each time point, addition of extracts obtained from either 5 or 10 mg empty NPs did not significantly change cell viability compared to control group (Figure 5c). In addition, increase in cell viability was observed with time indicating that cells proliferated.

3.11 | Effect of bFGF and TGF-β1 Released from PLGA NPs on DPSCs

The effect of bFGF loaded NPs prepared with different excipients on cell viability was investigated using eluates obtained of NPs in low glucose medium. On Day 1, cell viability in all groups was similar; afterwards cell viability in all groups was significantly higher than observed in control group (Figure 5d). Heparin 0.5% group showed significant difference in cell viability compared to experimental groups at fourth day; however, this difference was not significant at seventh and 11th days. For evaluation of TGF-β1 release from PLGA NPs, only two excipients of heparin and Kolliphor P 188 were used. Cell viability measured for heparin 1.0% group was significantly higher than observed in other groups on days 7 and 11 (Figure 5e). A time dependent increase in cell viability was observed for this group indicating that TGF-β1 has proliferative effect on DPSCs. Therefore, using 1.0% heparin was chosen as excipient for preparing TGF-β1 loaded NPs.

3.12 | Cell viability in hydrogels

Hydrogels with different compositions were used to determine the most suitable candidates for DPSCs viability. Significant increase in cell viability was observed in PEG10, PEG10-SF8 (3:1) and (1:1) groups at the end of seventh day, while no significant change in cell viability was observed for other groups (Figure 6a). PEG10-SF8(1:1) had moderate compressive modulus (185.35 ± 31.33 kPa) and degradation rate (37.21 ± 5.15%) at the end of 28 days compared to other blend hydrogels (Figures 3a and S2, respectively); however, elasticity of the PEG10-SF8(1:1) group was slightly higher than the elasticity of the scaffolds reported in literature to direct stem cell differentiation for cartilage tissue (Han, Zhu, Guo, Yang, & Li, 2016). Since highest cell viability was observed in PEG10-SF8(1:1) hydrogel this group was chosen for investigating the effect of GFs released from NPs on viability of DPSCs.

3.13 | Viability of DPSCs entrapped in hydrogels containing PLGA NPs

Viability of DPSCs in hydrogels containing PLGA NPs was measured by Alamar Blue and monitored by live/dead assay. bFGF and TGF-β1 loaded PLGA NPs with 0.5 and 1.0% heparin excipient have been used, respectively. Hydrogels without NPs and hydrogels containing empty NPs (2.5 mg/ml) were used as two control groups. Alamar Blue assay results showed that there was no significant difference between empty hydrogels and hydrogels with empty NPs, which indicated that there was no cytotoxic effect of NPs (Figure 6b). Cell viability in GF loaded NPs containing groups, was indifferent of empty NPs on first

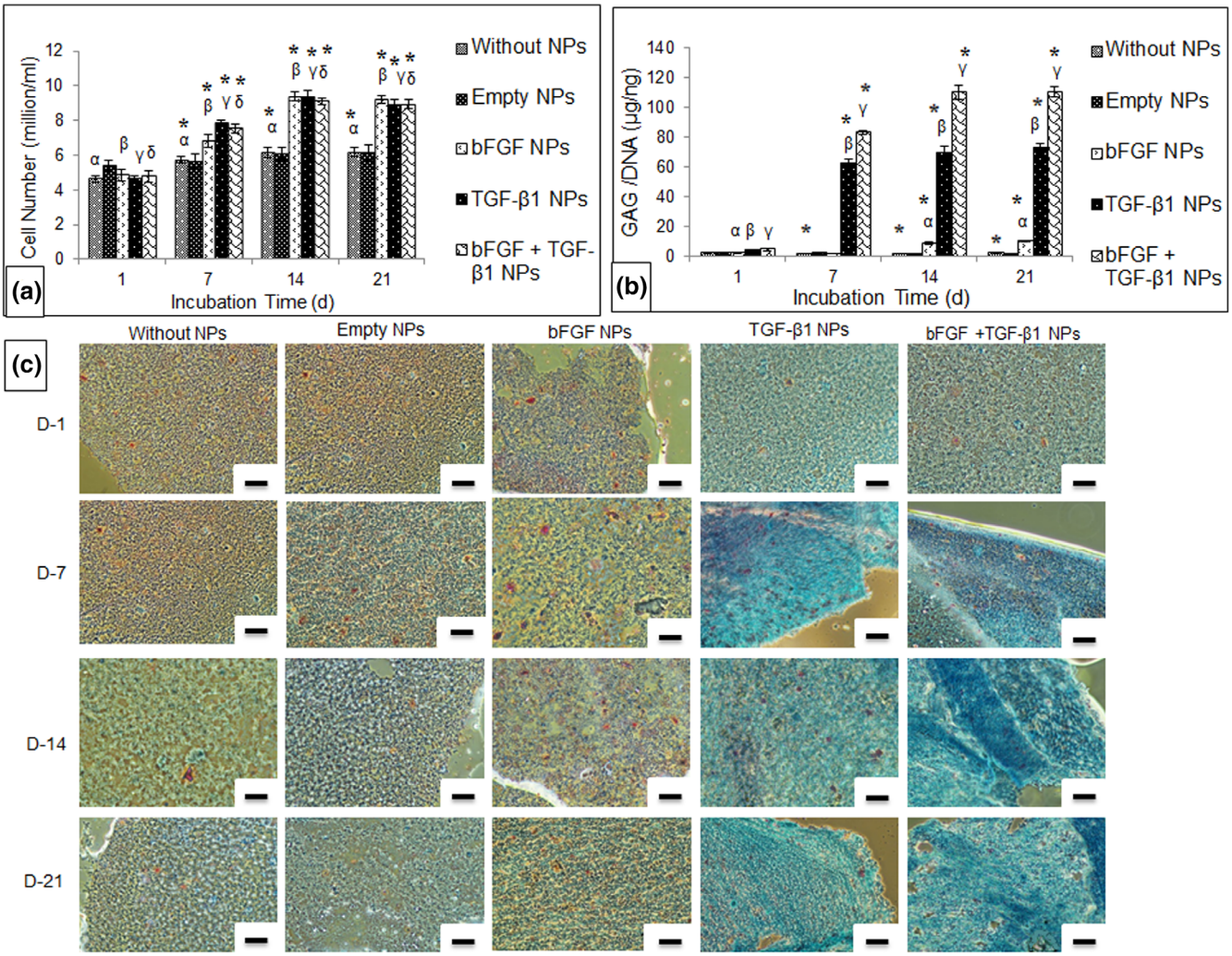

FIGURE 7 Proliferation of DPSCs in (a) and GAG content of (b) PEG10-SF8(1:1) hydrogels with NPs. Alcian Blue staining images for sulfated proteoglycans deposition (c). Intensity of blue color shows strongly acidic sulfated proteoglycans production by the cells; nuclear fast red was used to counterstain nuclei (pink to red) and cytoplasm (pale pink) of DPSCs (10× magnification, scale bar = 100 μm). α, β, γ, and δ show significant difference between results of day and other incubation days ($p \leq .05$). *Statistically significant differences between without NPs group and experimental groups at the same day ($p \leq .05$)

day. However, at seventh day, cell viability was significantly higher in 3 GF bearing hydrogel groups compared to hydrogel groups with empty NPs and without NPs. No significant difference was observed among these 3 GF bearing hydrogel groups. At 14th day, cell viability significantly increased in the groups containing both bFGF loaded NPs and TGF-β1 loaded NPs which indicated their synergistic effect on viability of DPSCs. In the other two groups containing GF loaded GFs of one type; cell viability was higher than observed in empty NPs and without NPs groups at 14th day. At 21st day cell viability in hydrogels containing bFGF and TGF-β1 loaded NPs remained constant which was the highest among all groups, The confocal image analysis for live/dead assay showed that cell density almost remained same until the first week in the two control groups but it slightly increased at the end of second and third weeks (Figure 6c). For bFGF loaded NPs containing group, cell number significantly increased at the end of seventh day and remained almost constant until the end of third week. Additionally, cells kept their spherical morphology. Cell number in the TGF-β1 group increased at first week and cells had elongated morphology; however, some dead cells were also observed in the confocal images. Cells in bFGF NPs and TGF-β1 NPs containing group increased in number with time and their morphology was elongated. Additionally, in this group, fewer dead cells were observed compared to alone TGF-β1 NPs containing group.

3.14 | DNA quantification in DPSCs encapsulated hydrogels

Cell number inside hydrogels which contained NPs and DPSCs was determined through DNA quantitation using Hoechst dye and conversion into cell number (7.0 pg/cell; Cui & Irudayaraj, 2015). Change in cell number was examined to study the effect of NPs on cell proliferation. Cellular proliferation in hydrogel groups containing GF loaded NPs was significantly higher than other groups on seventh day

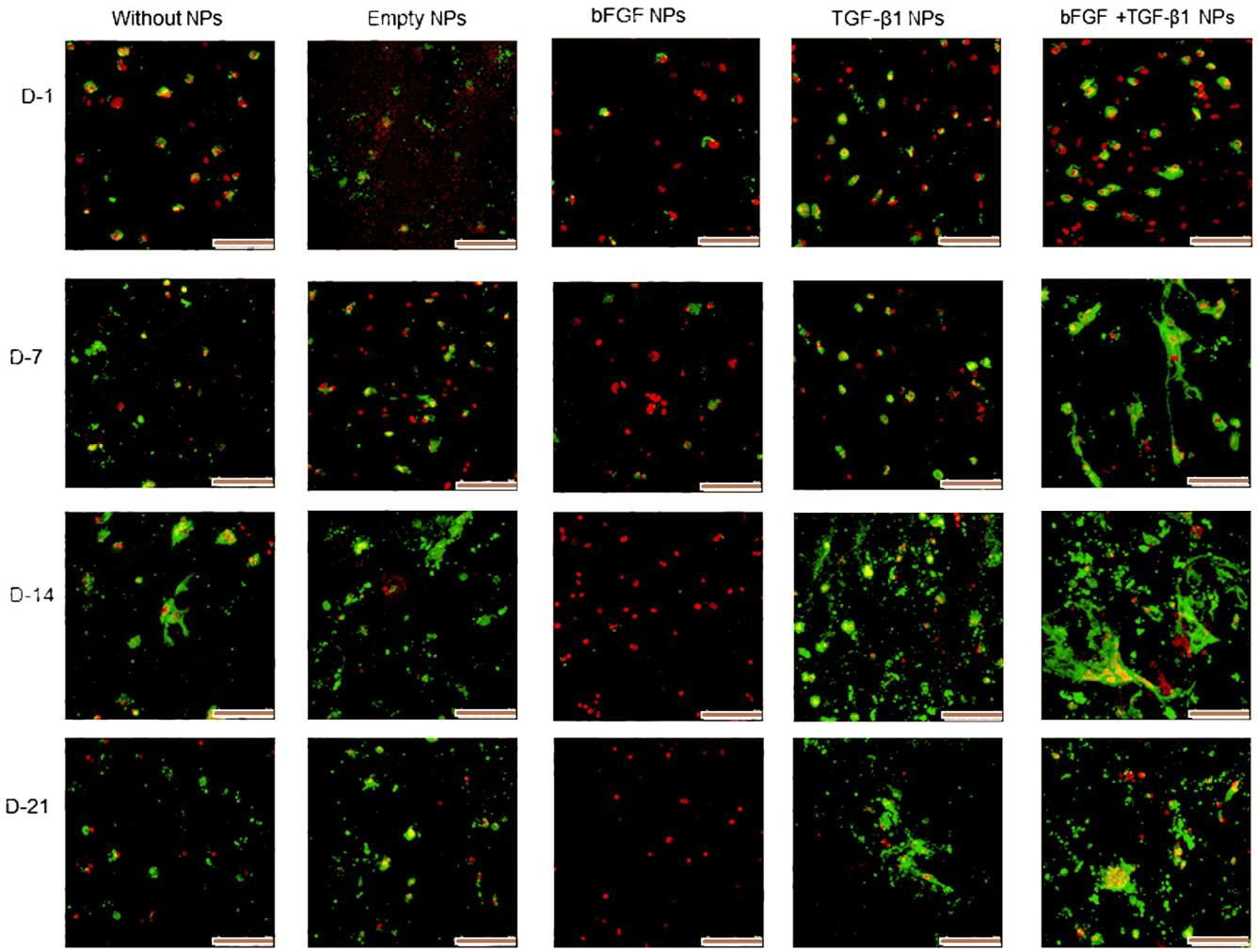

FIGURE 8 Immunohistochemical analysis of collagen type II deposition by the cells in PEG10-SF8 (1:1) hydrogels. Anti-collagen type II (green) antibody was used to stain collagen and nuclei of DPSCs were stained with DRAQ5 (red; 40× magnification, scale bar = 75 μm)

(Figure 7a). Cellular proliferation in hydrogels with NPs loaded GF increased until seventh day and remained same after seventh day which was in accordance with Alamar Blue assay results. For the other three GF containing groups, higher cellular proliferation also matched with higher cell viability obtained in Alamar blue assay.

3.15 | Determination of total sulfated glycosaminoglycan content of hydrogels

Total sulfated GAG content of hydrogels, an important indicator of chondrogenic differentiation, that were produced by cells was determined in hydrogels containing NPs by DMMB assays in cell lysates obtained during DNA quantitation assay. GAG content was normalized with DNA amount (μg/ng). GAG content of hydrogels without NPs and empty NPs groups remained constant during 21 days of incubation (Figure 7b). Significant increase in GAG content of the hydrogels containing bFGF loaded NPs was observed from on first day to 21st (from 2.35 ± 0.17 to 10.12 ± 0.42 μg/ng). For TGF-β1 NPs bearing groups increase in GAG production was also significant from Day 1 (4.00 ± 0.75 μg/ng) to the day 21 (72.95 ± 2.71 (μg/ng)). bFGF + TGF-β1 NPs bearing hydrogel group showed the most significant increase in GAG amount from 4.81 ± 1.08 (μg/ng) on first day to 110.35 ± 3.66 (μg/ng) on 21st day. At the end of 21 days, GAG content of hydrogels containing bFGF + TGF-β1 NPs was significantly higher than observed in other groups. Similar results in which covalently tethered TGF-β1 in PEGDA hydrogels were used for entrapment of human MSCs were reported. GAG/DNA content of the hydrogels went up to 70.20 ± 5.60 μg/ng (McCall, Luoma, & Anseth, 2012). It can be deduced that synergistic effect of both GFs on chondrogenic differentiation provided better cartilage specific ECM deposition (higher GAG production).

3.16 | Alcian blue staining for Sulfated proteoglycans in hydrogels

Alcian Blue staining was done to observe sulfated proteoglycans produced by cells. While no sulfated proteoglycans can be seen in the sections of hydrogels on the first day in groups without TGF-β1

loaded NPs, two TGF-β1 loaded NPs containing hydrogel groups showed very pale blue staining (Figure 7c). At seventh day both control and bFGF loaded NPs containing groups showed almost no sulfated proteoglycans staining while the production of sulfated proteoglycans can be observed in groups containing the TGF-β1 (observed as intense blue color in the vicinity of cells). The intensity of blue color in TGF-β1 + bFGF NPs containing group was higher compared to only TGF-β1 NPs containing group at seventh day. Staining intensity for sulfated proteoglycans increased with time. At 14th and 21st days small amount of sulfated proteoglycans production was observed in control and bFGF NPS containing groups.

3.17 | Immunohistochemical analysis

Collagen type II is the main fibrillar component of ECM in articular cartilage and plays crucial role in maintaining the ECM structure. Collagen type II production in hydrogels was studied with immunohistochemical analysis (Figure 8). Staining results indicated the presence of intracellular collagen on the 1st day in hydrogel groups containing empty NPs and without NPs groups. While decrease in deposition of collagen can be seen in bFGF NPs bearing group, relative higher deposition was observed in TGF-β1 NPs and bFGF NPs + TGF-β1 NPs groups compared to control groups. Interestingly, increase in deposition of collagen was observed in control groups at 7th, 14th, and 21st days indicating the capacity of the hydrogels to enhance collagen type II secretion. For the bFGF NPs group decrease in deposition of collagen type II synthesis was observed on days 7, 14 and 21, which was in accordance with literature (Khan et al., 2018). For TGF-β1 NPs bearing group enhancement of collagen type II production was seen on other days but the intensity of collagen deposition is not as high as bFGF NPs + TGF-β1 NPs group.

4 | DISCUSSION

Trauma, diseases, and age-related factors can trigger articular cartilage degeneration especially in knee leading to severe pain and eventually limited mobility of the patients. For successful cartilage regeneration a microenvironment which is stable during the healing process and inductive to chondrogenic differentiation is required. In this study, a hydrogel based microenvironment containing GF loaded nanoparticles was developed for stem cell delivery and their chondrogenic differentiation for articular cartilage regeneration.

Zeta potential indicates the potential difference between the dispersion medium and the stationary layer of fluid attached to the dispersed particle (Honary & Zahir, 2013). Physicochemical properties of the PLGA NPs depend on their charge and play critical role in the interaction of NPs with cells, especially for cellular uptake (Yameen et al., 2014). Generally, NPs are reported to be stable when the absolute value of the zeta potential is more than 30 mV (Lasoń, Sikora, & Ogonowski, 2013); consequently, it can be deduced that PLGA NPs prepared will remain in a stable colloidal condition. Various factors including formulation, type of surfactant and polymers, and their concentration can influence the zeta potential. In literature, different charge distribution has been reported (Sadat, Jahan, & Haddadi, 2016; Tefas, Tomuta, Achim, & Vlase, 2015). Patil, Sandberg, Heckert, Self, and Seal (2007) reported that NPs with a charge of −43 mV had the highest cellular uptake compared to NPs with less negative charge or positive charge. PLGA NPs we produced had lower negative charge (−27.10 ± 8.40 mV) compared to the values reported in literature (Figure 1b). However size of the NPs is suitable for cellular uptake as reported in the literature (Wang et al., 2018). On the other hand, lower negative charge of NPs will decrease cellular uptake of PLGA NPs which would favor GF release within ECM; consequently, it would help binding of GFs upon release from NPs to their receptor on plasma membrane. Size of NPs determined from SEM images (Figure 1c) and zeta size analysis (Figure 1d) revealed that particles produced were nanosized. SEM images showed a submicron size distribution for NPs (Figure 1a). Filtering of particles can be applied to provide more homogeneous and small size particle distribution, as the large size particles (≥500 nm) can represent significant particle mass in the sample and consequently effect the release profile of GFs. Encapsulation of bFGF in the PLGA NPs showed similar characteristic with empty PLGA NPs in morphology, size, and surface charge features (Figure S1). No significant change was observed in the mentioned parameters after encapsulation of bFGF. Co-encapsulation of vascular endothelial growth factor (VEGF) and bFGF in PLGA NPs which were prepared by modified solvent diffusion technique was reported (Losi et al., 2013). Similarly, no significant change in the particle size was reported between unloaded and loaded NPs.

In this study, effect of two different excipients, heparin and Kolliphor P 188, on in vitro release profile of bFGF and TGF-β1 was studied. EE of the bFGF ranged from 80.12 ± 0.41% to 94.70 ± 0.21% depending on the type and concentration of the excipient. Similar high EE (95%) was reported for bFGF encapsulated in the PLGA NPs (Losi et al., 2013). Si Zhu et al. observed that addition of heparin to bFGF loaded PLGA millicylinder has increased cumulative release from 1.9 ± 1.3% to 71 ± 5% (Zhu, Mallery, & Schwendeman, 2000), but concentration dependent effect of heparin in PLGA millicylinder was not reported in that study. bFGF was reported to have high affinity to heparin and upon binding heparin protects bFGF from denaturation and protease degradation (Meneghetti et al., 2015). Mechanism of binding was reported to be mediated by ionic interactions between both 2-O-sulfate groups and N-sulfate groups of heparin molecules and certain lysine (Lys^+) and arginine (Arg^+) cations in proteins and peptides (Rusnati et al., 1994). Therefore, increasing the heparin concentration as excipient from 0.1% to 0.5% (W/V) can cause the formation of clusters and provide a more protective effect as binding force becomes stronger. While cluster formation would increase release of bFGF, further increase in concentration of heparin to 1.0% (W/V) could also limit the complete release of the bFGF from PLGA NPs (Figure 2a,b). Heparin also has affinity to TGF-β1 and it has been reported that it binds directly to TGF-β1 (Rider & Mulloy, 2017). Therefore, similar to bFGF, concentration-dependent behavior of heparin was observed for TGF-β1. As the concentration of heparin was

increased higher amounts were released during burst release which was also followed with higher cumulative release (Figure 2a,b).

Kinetic model evaluation of GFs release based on the experimental data revealed Korsmeyer–Peppas model was best fitted for both GFs (Tables S4 and S5). As the n value for both GFs was less than 0.43 Fickian or quasi-Fickian diffusion from NPs was observed (Siepmann & Siepmann, 2008). In Fickian diffusion, the rate of penetrant diffusion dominates the kinetics and as the erosion of polymer (PLGA) had no effect on release, release of GFs was fast (Foreman & Vollmer, 2015; Holowka & Bhatia, 2014). Consequently, independent of the NPs erosion an effective dose of GFs for both proliferation and differentiation purposes will be released from PLGA NPs in a short period of time.

Presence of semi-degradable system based on SF and PEGDMA can provide a versatile platform for modulating mechanical properties of scaffolds for wide range of applications with wide range of compressive modulus (Figure 3a). In blend hydrogels, increasing the concentration of PEGDMA from 10% to 20%, caused a significant increase in the compressive strength of the hydrogels (Figure 3b). Thus, mechanical properties of the hydrogel were found predominantly to be related to the PEG concentration. Mechanical properties of scaffolds can be influenced through incorporation of NPs. a decrease in compressive modulus of hydrogels was observed in pure SF8 group. This could be due to prevention of β-sheet formation in the presence of NPs within the fibroin matrix. Similarly, incorporation of NPs such as hydroxyapatite NPs in SF hydrogel was reported to decrease the compressive load due to lack of interaction between NPs and SF (Kim et al., 2017). However, for blend hydrogels with exception of PEG15-SF8 (1:3) group incorporation of PLGA NPs did not significantly change the compressive strength (Figure 3d). Hydrogels showed diverse swelling ratio and (Figure S3) and weight loss (Figure S4) depending on their composition. Generally, higher concentration of hydrogels component can lead to a tighter structure which leads to a decrease in mesh size of polymeric network and consequently lower uptake capacity (Haraguchi, Farnworth, Ohbayashi, & Takehisa, 2003). Decrease in PEGDMA content of blend hydrogels, resulted in decreased swelling ratio. Decrease in the swelling ratio can be due to lesser content of PEGDMA and degradation of fibroin within the hydrogel matrix which consequently led to a decrease in swelling ratio. Less than 20% weight loss in PEGDMA could be due to their chemical crosslinking nature. Poly(ether) back bone of PEGDMA was reported to be resistant to hydrolytic degradation (Browning, Cereceres, Luong, & Cosgriff-Hernandez, 2014). Degradation of fibroin starts with the hydrophilic blocks of fibroin and after that, hydrophobic crystal blocks that were formerly surrounded and immobilized by hydrophilic blocks become free particles and move into solution (Lu et al., 2011). Therefore, lower content of both hydrophilic blocks and hydrophobic crystal blocks can lead to faster degradation of SF4 group compared to SF8. In blend hydrogels, lower PEGDMA concentration led to a higher degradation rate. No significant difference in weight loss was observed for enzymatic degradation of hydrogels in 10 μg/ml lysozyme enzyme solution in PBS (Figure S5). This concentration resembles the enzyme concentration in synovial fluid of damaged articular cartilage tissue such as osteoarthritis condition (Pruzanski, Saito, & Ogryzlo, 1970). Consequently, it can be deduced that hydrogels will show similar degradation profile in the presence of lysozyme when implanted.

Chemical characterization of hydrogels using FTIR confirmed PEGDMA photopolymerization and SF physical crosslinking (Figure 4a,b). The characteristic peaks for both PEGDMA and SF were not changed during the gelation process and no new specific peaks were seen in the spectra of blend hydrogels; consequently, no covalent bond was formed between these two polymers. Morphological analysis of hydrogels using SEM analysis showed highly interconnected pore structure with various pore size distributions (Figure 4c). Pore size plays a critical role in cell attachment and migration, morphology and gene expression (Ji et al., 2011; Kuberka et al., 2002; O'Brien et al., 2007). MSCs were reported to prefer larger pore sizes (e.g., 300 μm) which significantly provide higher cell proliferation, chondrogenic gene expression, cartilage-like matrix deposition (Matsiko, Gleeson, & O'Brien, 2014). As pore size distribution in blend hydrogels such as PEG10-SF8(3:1) and (1:1) groups ranged between 40 and 400 μm, it could be one of the important reasons for high cell viability of DPSCs in these groups (Figure S6). Therefore, these blend hydrogels can provide suitable pore size and interconnectivity suitable for chondrocyte activities and consequently, they are good candidates for cartilage TE applications.

Cytotoxicity test of empty PLGA NPs conducted using DPSCs indicated that viability of cells was not significantly affected by NPs (Figure 5c). Therefore, PLGA NPs can be used safely without any safety concerns. In this study, effect of bFGF and TGF-β1 on cell viability was investigated (Figure 7d,e). bFGF could play crucial role in maintaining the undifferentiated state of adult stem cells through inducing their proliferative and self-renewal capacity (Nawrocka, Kornicka, Szydlarska, & Marycz, 2017). TGF-β1 possess key regulatory effect in chondrocyte proliferation (Park et al., 2005). Therefore, effect of heparin and Kolliphor P 188 as excipient in GFs bearing PLGA NPs on DPSCs viability was studied. bFGF and TGF-β1 0.5% heparin and 1.0% heparin bearing groups demonstrated the highest cell viability, respectively. Heparin has high affinity to bind to the bFGF; therefore, increasing the concentration of the heparin as an excipient from 0.1% to 0.5% (W/V) can cause the formation of clusters of bFGF that will lead to much stronger binding force and consequently, which would protect the bFGF from degradation and as a result cell viability increased compared to 0.1% heparin bearing group (Rusnati et al., 1994). However, as the concentration was increased to 1.0%, release of GF might have decreased due to high interaction and much more cluster formation between bFGF and heparin which might have led to a plateau value that prevented the positive effect of bFGF on DPSCs. Proliferation of DPSCs is desired to be fast during first days; therefore, 0.5% heparin group which showed the highest cell viability on fourth day was chosen for preparing bFGF loaded PLGA NPs.

For choosing most suitable hydrogel composition, viability of entrapped DPSCs within hydrogels was determined and highest cell viability was observed in PEG10-SF8(1:1) group (Figure 6a).

PEG10-SF8(1:1) had moderate compressive modulus (185.35 ± 31.33 kPa) and degradation rate (37.21 ± 5.15%) at the end of 28 days compared to other blend hydrogels (Figures 3a and S2, respectively); however, elasticity of the PEG10-SF8(1:1) group was slightly higher than the elasticity of the scaffolds reported in literature to direct stem cell differentiation for cartilage tissue (Han et al., 2016). Since highest cell viability was observed in PEG10-SF8(1:1) hydrogel group, it was chosen for investigating the effect of GFs released from NPs on viability of DPSCs. Afterwards, effect of PLGA NPs on viability of DPSCs within PEG10-SF8(1:1) hydrogels was investigated (Figure 6b). Similar to monolayer study, within the hydrogel no cytotoxic effect of empty PLGA NPs on DPSCs was observed. High cellular viability at the end of 14th day for bFGF NPs + TGF-β1 NPs group indicated their synergistic effect of these two GFs on viability of DPSCs compared to their single effect. Confocal images (Figure 6c) and DNA amounts (Figure 7a) were also in accordance with the cell viability results, where cell number significantly increased in bFGF NPs + TGF-β1 NPs group. DMMB assay was used for determination of total sulfated GAG content of the hydrogels (Figure 7b). At the end of 21 days, GAG content of hydrogels containing bFGF NPs + TGF-β1 NPs group (110.35 ± 3.66 μg/ng) was significantly higher than observed in other groups. Similar results were reported in which covalently tethered TGF-β1 in PEGDA hydrogels were used for entrapment of human MSCs and GAG/DNA content up to 70.20 ± 5.60 μg/ng (McCall et al., 2012). It can be deduced that synergistic effect of both GFs on chondrogenic differentiation provided better cartilage specific ECM deposition (higher GAG production). Alcian Blue staining of sulphated proteoglycans as indicator of chondrogenic differentiation of DPSCs was evaluated (Figure 7c). While only TGF-β1 bearing groups were stained for sulfated proteoglycans but staining and consequently, production of sulphated proteoglycans was more intense in bFGF NPs + TGF-β1 NPs group on seventh day. To evaluate the collagen type II production which is the main fibrillar component of ECM in articular cartilage and plays crucial role in maintaining the ECM structure immunohistochemical analysis was performed (Figure 8). Collagen type II staining was observed in TGF- β1 groups but more staining, in other words higher production was observed in bFGF NPs + TGF-β1 NPs group. Consequently, synergistic effect of two GFs was shown by higher deposition of extracellular and intracellular collagen type II in the scaffolds at Day 14.

5 | CONCLUSION

In this study, SF and of poly(ethylene glycol) dimethacrylate (PEGDMA) were used to provide a versatile platform for preparing hydrogels with tunable mechanical, swelling and degradation properties through physical and chemical crosslinking as a microenvironment for chondrogenic differentiation in the presence of bFGF and TGF-β1 releasing nanoparticles Simultaneous delivery of bFGF and TGF-β1 as two key GFs in articular cartilage improved viability and proliferation of stem cells as well as chondrogenic differentiation in terms of higher GAG and collagen type II production compared to only one type of GF delivery. Our results suggest that by incorporation of NPs into such hydrogels, it was possible to obtain cost effective, dosage- and site-specific delivery of relevant GFs for cartilage tissue regeneration.

ACKNOWLEDGEMENTS

We would like to thank METU BAP (project NO: GAP-310-2018-2847), Horizon 2020 PANBioRA (760921) project, Center of Excellence in Biomaterials and Tissue Engineering (BIOMATEN) for their supports.

CONFLICT OF INTEREST

There is no conflict of interest to declare.

REFERENCES

Akmal, M. N., Zarina, Z. I., Rohaya, M., Sahidan, S., Zaidah, Z., & Hisham, Z. S. (2014). Isolation and characterization of dental pulp stem cells from murine incisors. *Journal of Biological Sciences*, *14*(4), 327–331.

Alexis, F., Pridgen, E., Molnar, L. K., & Farokhzad, O. C. (2008). Factors affecting the clearance and biodistribution of polymeric nanoparticles. *Molecular Pharmaceutics*, *5*(4), 505–515.

Alford, J. W., & Cole, B. J. (2005). Cartilage restoration, part 1: Basic science, historical perspective, patient evaluation, and treatment options. *The American Journal of Sports Medicine*, *33*(2), 295–306.

Allison, S. D. (2008). Analysis of initial burst in PLGA microparticles. *Expert Opinion on Drug Delivery*, *5*(6), 615–628.

Altman, G. H., Diaz, F., Jakuba, C., Calabro, T., Horan, R. L., Chen, J., … Kaplan, D. L. (2003). Silk-based biomaterials. *Biomaterials*, *24*(3), 401–416.

Barry, F., Boynton, R. E., Liu, B., & Murphy, J. M. (2001). Chondrogenic differentiation of Mesenchymal stem cells from bone marrow: Differentiation-dependent gene expression of matrix components. *Experimental Cell Research*, *268*(2), 189–200.

Bertassoni, L. E., Cardoso, J. C., Manoharan, V., Cristino, A. L., Bhise, N. S., Araujo, W. A., … Dokmeci, M. R. (2014). Direct-write bioprinting of cell-laden methacrylated gelatin hydrogels. *Biofabrication*, *6*(2), 024105.

Bobo, D., Robinson, K. J., Islam, J., Thurecht, K. J., & Corrie, S. R. (2016). Nanoparticle-based medicines: A review of FDA-approved materials and clinical trials to date. *Pharmaceutical Research*, *33*(10), 2373–2387.

Bock, N., Dargaville, T. R., & Woodruff, M. A. (2014). Controlling microencapsulation and release of micronized proteins using poly(ethylene glycol) and electrospraying. *European Journal of Pharmaceutics and Biopharmaceutics*, *87*(2), 366–377.

Boehnke, N., Kammeyer, J. K., Damoiseaux, R., & Maynard, H. D. (2018). Stabilization of glucagon by Trehalose Glycopolymer Nanogels. *Advanced Functional Materials*, *28*(10), 1705475.

Brittberg, M., Lindahl, A., Nilsson, A., Ohlsson, C., Isaksson, O., & Peterson, L. (1994). Treatment of deep cartilage defects in the knee with autologous chondrocyte transplantation. *The New England Journal of Medicine*, *331*(14), 889–895.

Browning, M., Cereceres, S., Luong, P., & Cosgriff-Hernandez, E. (2014). Determination of the in vivo degradation mechanism of PEGDA hydrogels. *Journal of Biomedical Materials Research, Part A*, *102*(12), 4244–4251.

Buckwalter, J., & Mankin, H. (1998). Articular cartilage: Tissue design and chondrocyte-matrix interactions. *Instructional Course Lectures*, *47*, 477–486.

Buckwalter, J. A. (1998). Articular cartilage: Injuries and potential for healing. *The Journal of Orthopaedic and Sports Physical Therapy*, *28*(4), 192–202.

Bystroňová, J., Ščigalková, I., Wolfová, L., Pravda, M., Vrana, N. E., & Velebný, V. (2018). Creating a 3D microenvironment for monocyte cultivation: ECM-mimicking hydrogels based on gelatine and hyaluronic acid derivatives. *RSC Advances*, *8*(14), 7606–7614.

Caplan, A. I. (1999). *Embryonic development and the principles of tissue engineering. 2003* (pp. 17–24). Chichester, NY: Wiley.

Chia, S. L., Sawaji, Y., Burleigh, A., McLean, C., Inglis, J., Saklatvala, J., & Vincent, T. (2009). Fibroblast growth factor 2 is an intrinsic chondroprotective agent that suppresses ADAMTS-5 and delays cartilage degradation in murine osteoarthritis. *Arthritis and Rheumatism*, *60* (7), 2019–2027.

Chubinskaya, S., & Rueger, D. C. (2017). BMP Signaling in articular cartilage repair and regeneration: Potential therapeutic opportunity for osteoarthritis. In S. Vukicevic & K. Sampath (Eds.), *Bone Morphogenetic Proteins: Systems Biology Regulators* (pp. 171–185). Cham: Springer.

Crisan, M., Yap, S., Casteilla, L., Chen, C.-W., Corselli, M., Park, T. S., … Péault, B. (2008). A perivascular origin for Mesenchymal stem cells in multiple human organs. *Cell Stem Cell*, *3*(3), 301–313.

Cui, Y., & Irudayaraj, J. (2015). Inside single cells: Quantitative analysis with advanced optics and nanomaterials. *Wiley Interdisciplinary Reviews. Nanomedicine and Nanobiotechnology*, *7*(3), 387–407.

Dash, S., Murthy, P. N., Nath, L., & Chowdhury, P. (2010). Kinetic modeling on drug release from controlled drug delivery systems. *Acta Poloniae Pharmaceutica*, *67*(3), 217–223.

Di Benedetto, A., Carbone, C., & Mori, G. (2014). Dental pulp stem cells isolation and osteogenic differentiation: A good promise for tissue engineering. In C. Kioussi (Ed.), *Stem Cells and Tissue Repair* (pp. 117–130). New York, NY: Springer.

Ertan, A. B., Yilgor, P., Bayyurt, B., Calikoglu, A. C., Kaspar, C., Kok, F. N., … Hasirci, V. (2013). Effect of double growth factor release on cartilage tissue engineering. *Journal of Tissue Engineering and Regenerative Medicine*, *7*(2), 149–160.

Fathi-Achachelouei, M., Knopf-Marques, H., Riberio de Silva, C. E., Barthès, J. G. D., Bat, E., Tezcaner, A., & Vrana, N. E. (2019). Use of nanoparticles in tissue engineering and regenerative medicine. *Frontiers in Bioengineering and Biotechnology*, *7*, 113.

Foreman, M. R., & Vollmer, F. (2015). Optical tracking of anomalous diffusion kinetics in polymer microspheres. *Physical Review Letters*, *114*(11), 118001.

Fröhlich, K., Hartzke, D., Schmidt, F., Eucker, J., Gurlo, A., Sittinger, M., & Ringe, J. (2018). Delayed release of chemokine CCL25 with bioresorbable microparticles for mobilization of human mesenchymal stem cells. *Acta Biomaterialia*, *69*, 290–300.

Grafe, I., Alexander, S., Peterson, J. R., Snider, T. N., Levi, B., Lee, B., & Mishina, Y. (2018). TGF-β family signaling in mesenchymal differentiation. *Cold Spring Harbor Perspectives in Biology*, *10*(5), a022202.

Han, F., Zhu, C., Guo, Q., Yang, H., & Li, B. (2016). Cellular modulation by the elasticity of biomaterials. *Journal of Materials Chemistry B*, *4* (1), 9–26.

Hangody, L., Feczkó, P., Bartha, L., Bodó, G., & Kish, G. (2001). Mosaicplasty for the treatment of articular defects of the knee and ankle. *Clinical Orthopaedics and Related Research*, *391*, S328–S336.

Haraguchi, K., Farnworth, R., Ohbayashi, A., & Takehisa, T. (2003). Compositional effects on mechanical properties of nanocomposite hydrogels composed of poly (N, N-dimethylacrylamide) and clay. *Macromolecules*, *36*(15), 5732–5741.

Holowka, E. P., & Bhatia, S. K. (2014). Controlled-release systems. In E. P. Holowka & S. K. Bhatia (Eds.), *Drug Delivery: Materials Design and Clinical Perspective* (pp. 7–62). New York, NY: Springer.

Honary, S., & Zahir, F. (2013). Effect of zeta potential on the properties of nano-drug delivery systems-a review (part 1). *Tropical Journal of Pharmaceutical Research*, *12*(2), 255–264.

Huang, G.-J., Gronthos, S., & Shi, S. (2009). Mesenchymal stem cells derived from dental tissues vs. those from other sources: Their biology and role in regenerative medicine. *Journal of Dental Research*, *88*(9), 792–806.

Hwang, J. W., Noh, S. M., Kim, B., & Jung, H. W. (2015). Gelation and crosslinking characteristics of photopolymerized poly (ethylene glycol) hydrogels. *Journal of Applied Polymer Science*, *132*(22), 41939.

James, C.-B., & Uhl, T. L. (2001). A review of articular cartilage pathology and the use of glucosamine sulfate. *Journal of Athletic Training*, *36*(4), 413–419.

Ji, C., Khademhosseini, A., & Dehghani, F. (2011). Enhancing cell penetration and proliferation in chitosan hydrogels for tissue engineering applications. *Biomaterials*, *32*(36), 9719–9729.

Jung, Y., Chung, Y.-I., Kim, S. H., Tae, G., Kim, Y. H., Rhie, J. W., … Kim, S. H. (2009). In situ chondrogenic differentiation of human adipose tissue-derived stem cells in a TGF-β1 loaded fibrin–poly(lactide-caprolactone) nanoparticulate complex. *Biomaterials*, *30*(27), 4657–4664.

Kayabolen, A., Keskin, D., Aykan, A., Karslıoglu, Y., Zor, F., & Tezcaner, A. (2017). Native extracellular matrix/fibroin hydrogels for adipose tissue engineering with enhanced vascularization. *Biomedical Materials*, *12*(3), 035007.

Khan, S., Muhammad, H., Scammahorn, J., Dell'Accio, F., & Vincent, T. (2018). Fibroblast growth factor 2 promotes regeneration of cartilage by attracting mesenchymal stem cells to the site of cartilage injury. *Osteoarthritis and Cartilage*, *26*, S37.

Killion, J. A., Geever, L. M., Devine, D. M., Kennedy, J. E., & Higginbotham, C. L. (2011). Mechanical properties and thermal behaviour of PEGDMA hydrogels for potential bone regeneration application. *Journal of the Mechanical Behavior of Biomedical Materials*, *4*(7), 1219–1227.

Kim, M. H., Kim, B. S., Lee, J., Cho, D., Kwon, O. H., & Park, W. H. (2017). Silk fibroin/hydroxyapatite composite hydrogel induced by gamma-ray irradiation for bone tissue engineering. *Biomaterials Research*, *21* (1), 12.

Kim, U.-J., Park, J., Li, C., Jin, H.-J., Valluzzi, R., & Kaplan, D. L. (2004). Structure and properties of silk hydrogels. *Biomacromolecules*, *5*(3), 786–792.

Kuberka, M., Von Heimburg, D., Schoof, H., Heschel, I., & Rau, G. (2002). Magnification of the pore size in biodegradable collagen sponges. *The International Journal of Artificial Organs*, *25*(1), 67–73.

Kubosch, E. J., Lang, G., Furst, D., Kubosch, D., Izadpanah, K., Rolauffs, B., … Schmal, H. (2018). The potential for synovium-derived stem cells in cartilage repair. *Current Stem Cell Research & Therapy*, *13*(3), 174–184.

Lasoń, E., Sikora, E., & Ogonowski, J. (2013). Influence of process parameters on properties of nanostructured lipid carriers (NLC) formulation. *Acta Biochimica Polonica*, *60*(4), 773–777.

Lee, K., Silva, E. A., & Mooney, D. J. (2011). Growth factor delivery-based tissue engineering: General approaches and a review of recent developments. *Journal of the Royal Society Interface*, *8*(55), 153–170.

Leisk, G. G., Lo, T. J., Yucel, T., Lu, Q., & Kaplan, D. L. (2010). Electrogelation for protein adhesives. *Advanced Materials*, *22*(6), 711–715.

Li, B., Davidson, J. M., & Guelcher, S. A. (2009). The effect of the local delivery of platelet-derived growth factor from reactive two-component polyurethane scaffolds on the healing in rat skin excisional wounds. *Biomaterials*, *30*(20), 3486–3494.

Li, X., Su, G., Wang, J., Zhou, Z., Li, L., Liu, L., … Wang, H. (2013). Exogenous bFGF promotes articular cartilage repair via up-regulation of multiple growth factors. *Osteoarthritis and Cartilage*, *21*(10), 1567–1575.

Lim, S. M., Oh, S. H., Lee, H. H., Yuk, S. H., Im, G. I., & Lee, J. H. (2010). Dual growth factor-releasing nanoparticle/hydrogel system for cartilage tissue engineering. *Journal of Materials Science. Materials in Medicine*, *21*(9), 2593–2600.

Lin, C.-C., & Anseth, K. S. (2009). PEG hydrogels for the controlled release of biomolecules in regenerative medicine. *Pharmaceutical Research*, *26* (3), 631–643.

Losi, P., Briganti, E., Errico, C., Lisella, A., Sanguinetti, E., Chiellini, F., & Soldani, G. (2013). Fibrin-based scaffold incorporating VEGF- and bFGF-loaded nanoparticles stimulates wound healing in diabetic mice. *Acta Biomaterialia*, *9*(8), 7814–7821.

Lu, Q., Zhang, B., Li, M., Zuo, B., Kaplan, D. L., Huang, Y., & Zhu, H. (2011). Degradation mechanism and control of silk fibroin. *Biomacromolecules*, *12*(4), 1080–1086.

Mata, M., Milian, L., Oliver, M., Zurriaga, J., Sancho-Tello, M., Llano, J. J. M., & Carda, C. (2017). In vivo articular cartilage regeneration using human dental pulp stem cells cultured in an alginate scaffold: A preliminary study. *Stem Cells International*, *2017*, 9.

Matsiko, A., Gleeson, J. P., & O'Brien, F. J. (2014). Scaffold mean pore size influences mesenchymal stem cell chondrogenic differentiation and matrix deposition. *Tissue Engineering Parts A*, *21*(3–4), 486–497.

McCall, J. D., Luoma, J. E., & Anseth, K. S. (2012). Covalently tethered transforming growth factor beta in PEG hydrogels promotes chondrogenic differentiation of encapsulated human mesenchymal stem cells. *Drug Delivery and Translational Research*, *2*(5), 305–312.

Mehta, P., Al-Kinani, A. A., Arshad, M. S., Chang, M.-W., Alany, R. G., & Ahmad, Z. (2017). Development and characterisation of electrospun timolol maleate-loaded polymeric contact lens coatings containing various permeation enhancers. *International Journal of Pharmaceutics*, *532*(1), 408–420.

Meneghetti, M. C., Hughes, A. J., Rudd, T. R., Nader, H. B., Powell, A. K., Yates, E. A., & Lima, M. A. (2015). Specific heparan sulfate saccharides mediate the activity of basic fibroblast growth factor. *Journal of the Royal Society Interface*, *12*(110), 20150589.

Mithoefer, K., Williams, R. J., III, Warren, R. F., Potter, H. G., Spock, C. R., Jones, E. C., … Marx, R. G. (2006). Chondral resurfacing of articular cartilage defects in the knee with the microfracture technique: Surgical technique. *Journal of Bone and Joint Surgery*, *88*, 294–304.

Moore, E., & West, J. (2018). Bioactive poly (ethylene glycol) acrylate hydrogels for regenerative engineering. *Regenerative Engineering and Translational Medicine*, *5*, 167–179.

Nawrocka, D., Kornicka, K., Szydlarska, J., & Marycz, K. (2017). Basic fibroblast growth factor inhibits apoptosis and promotes proliferation of adipose-derived Mesenchymal stromal cells isolated from patients with type 2 diabetes by reducing cellular oxidative stress. *Oxidative Medicine and Cellular Longevity*, *2017*, 3027109.

Nguyen, Q. T., Hwang, Y., Chen, A. C., Varghese, S., & Sah, R. L. (2012). Cartilage-like mechanical properties of poly (ethylene glycol)-diacrylate hydrogels. *Biomaterials*, *33*(28), 6682–6690.

Nikolaou, V. S., Chytas, D., & Babis, G. C. (2014). Common controversies in total knee replacement surgery: Current evidence. *World Journal of Orthopedics*, *5*(4), 460–468.

Nuttelman, C. R., Tripodi, M. C., & Anseth, K. S. (2004). In vitro osteogenic differentiation of human mesenchymal stem cells photoencapsulated in PEG hydrogels. *Journal of Biomedical Materials Research, Part A*, *68*(4), 773–782.

O'Brien, F. J., Harley, B. A., Waller, M. A., Yannas, I. V., Gibson, L. J., & Prendergast, P. J. (2007). The effect of pore size on permeability and cell attachment in collagen scaffolds for tissue engineering. *Technology and Health Care*, *15*(1), 3–17.

Park, H., Temenoff, J. S., Holland, T. A., Tabata, Y., & Mikos, A. G. (2005). Delivery of TGF-β1 and chondrocytes via injectable, biodegradable hydrogels for cartilage tissue engineering applications. *Biomaterials*, *26*(34), 7095–7103.

Park, J. S., Yang, H. N., Woo, D. G., Chung, H. M., & Park, K. H. (2009). In vitro and in vivo Chondrogenesis of rabbit bone marrow–derived stromal cells in fibrin matrix mixed with growth factor loaded in nanoparticles. *Tissue Engineering. Part A*, *15*(8), 2163–2175.

Patil, S., Sandberg, A., Heckert, E., Self, W., & Seal, S. (2007). Protein adsorption and cellular uptake of cerium oxide nanoparticles as a function of zeta potential. *Biomaterials*, *28*(31), 4600–4607.

Petros, R. A., & DeSimone, J. M. (2010). Strategies in the design of nanoparticles for therapeutic applications. *Nature Reviews Drug Discovery*, *9*, 615–627.

Pruzanski, W., Saito, S., & Ogryzlo, M. (1970). The significance of lysozyme (muramidase) in rheumatoid arthritis. I. Levels in serum and synovial fluid. *Arthritis and Rheumatism*, *13*(4), 389–399.

Ren, K., Cui, H., Xu, Q., He, C., Li, G., & Chen, X. (2016). Injectable polypeptide hydrogels with Tunable microenvironment for 3D spreading and Chondrogenic differentiation of bone-marrow-derived Mesenchymal stem cells. *Biomacromolecules*, *17*(12), 3862–3871.

Rider, C., & Mulloy, B. (2017). Heparin, heparan sulphate and the TGF-β cytokine superfamily. *Molecules*, *22*(5), 713.

Roberts, J. J., Earnshaw, A., Ferguson, V. L., & Bryant, S. J. (2011). Comparative study of the viscoelastic mechanical behavior of agarose and poly(ethylene glycol) hydrogels. *Journal of Biomedical Materials Research, Part B: Applied Biomaterials*, *99*(1), 158–169.

Rockwood, D. N., Preda, R. C., Yücel, T., Wang, X., Lovett, M. L., & Kaplan, D. L. (2011). Materials fabrication from *Bombyx mori* silk fibroin. *Nature Protocols*, *6*(10), 1612–1631.

Ruan, J.-L., Tulloch, N. L., Muskheli, V., Genova, E. E., Mariner, P. D., Anseth, K. S., & Murry, C. E. (2013). An improved cryosection method for polyethylene glycol hydrogels used in tissue engineering. *Tissue Engineering Part C*, *19*(10), 794–801.

Rusnati, M., Coltrini, D., Caccia, P., Dellera, P., Zoppetti, G., Oreste, P., … Presta, M. (1994). Distinct role of 2-O-, N-, and 6-O-Sulfate groups of heparin in the formation of the ternary complex with basic fibroblast growth factor and soluble FGF Receptor-1. *Biochemical and Biophysical Research Communications*, *203*(1), 450–458.

Sadat, S. M., Jahan, S. T., & Haddadi, A. (2016). Effects of size and surface charge of polymeric nanoparticles on in vitro and in vivo applications. *Journal of Biomaterials and Nanobiotechnology*, *7*(02), 91–108.

Sawaji, Y., Hynes, J., Vincent, T., & Saklatvala, J. (2008). Fibroblast growth factor 2 inhibits induction of aggrecanase activity in human articular cartilage. *Arthritis and Rheumatism*, *58*(11), 3498–3509.

Siepmann, J., & Siepmann, F. (2008). Mathematical modeling of drug delivery. *International Journal of Pharmaceutics*, *364*(2), 328–343.

Sophia Fox, A. J., Bedi, A., & Rodeo, S. A. (2009). The basic science of articular cartilage: Structure, composition, and function. *Sports Health*, *1*(6), 461–468.

Stewart, A. A., Byron, C. R., Pondenis, H., & Stewart, M. C. (2007). Effect of fibroblast growth factor-2 on equine mesenchymal stem cell monolayer expansion and chondrogenesis. *American Journal of Veterinary Research*, *68*(9), 941–945.

Tefas, L. R., Tomuta, I., Achim, M., & Vlase, L. (2015). Development and optimization of quercetin-loaded PLGA nanoparticles by experimental design. *Clujul Medical*, *88*(2), 214–223.

Vrana, N., Erdemli, O., Francius, G., Fahs, A., Rabineau, M., Debry, C., … Lavalle, P. (2014). Double entrapment of growth factors by nanoparticles loaded into polyelectrolyte multilayer films. *Journal of Materials Chemistry B*, *2*(8), 999–1008.

Wang, H., Agarwal, P., Zhao, S., Xu, R. X., Yu, J., Lu, X., & He, X. (2015). Hyaluronic acid-decorated dual responsive nanoparticles of Pluronic F127, PLGA, and chitosan for targeted co-delivery of doxorubicin and irinotecan to eliminate cancer stem-like cells. *Biomaterials*, *72*, 74–89.

Wang, X., Gao, J., Ouyang, X., Wang, J., Sun, X., & Lv, Y. (2018). Mesenchymal stem cells loaded with paclitaxel-poly(lactic-co-glycolic acid) nanoparticles for glioma-targeting therapy. *International Journal of Nanomedicine*, *13*, 5231–5248.

Wang, X., Kluge, J. A., Leisk, G. G., & Kaplan, D. L. (2008). Sonication-induced gelation of silk fibroin for cell encapsulation. *Biomaterials*, *29*(8), 1054–1064.

Wu, S.-C., Chen, C.-H., Wang, J.-Y., Lin, Y.-S., Chang, J.-K., & Ho, M.-L. (2018). Hyaluronan size alters chondrogenesis of adipose-derived stem cells via the CD44/ERK/SOX-9 pathway. *Acta Biomaterialia*, *66*, 224–237.

Yameen, B., Choi, W. I., Vilos, C., Swami, A., Shi, J., & Farokhzad, O. C. (2014). Insight into nanoparticle cellular uptake and intracellular targeting. *Journal of Controlled Release*, *190*, 485–499.

Ying, J., Wang, P., Zhang, S., Xu, T., Zhang, L., Dong, R., … Jin, H. (2018). Transforming growth factor-beta1 promotes articular cartilage repair through canonical Smad and hippo pathways in bone mesenchymal stem cells. *Life Sciences*, *192*, 84–90.

Yokota, J., Chosa, N., Sawada, S., Okubo, N., Takahashi, N., Hasegawa, T., … Ishisaki, A. (2014). PDGF-induced PI3K-mediated signaling enhances the TGF-β-induced osteogenic differentiation of human mesenchymal stem cells in a TGF-β-activated MEK-dependent manner. *International Journal of Molecular Medicine*, *33*(3), 534–542.

Yucel, T., Cebe, P., & Kaplan, D. L. (2009). Vortex-induced injectable silk fibroin hydrogels. *Biophysical Journal*, *97*(7), 2044–2050.

Zaharia, C., Tudora, M.-R., Stancu, I.-C., Galateanu, B., Lungu, A., & Cincu, C. (2012). Characterization and deposition behavior of silk hydrogels soaked in simulated body fluid. *Materials Science & Engineering, C: Materials for Biological Applications*, *32*(4), 945–952.

Zhang, Z., Li, L., Yang, W., Cao, Y., Shi, Y., Li, X., & Zhang, Q. (2017). The effects of different doses of IGF-1 on cartilage and subchondral bone during the repair of full-thickness articular cartilage defects in rabbits. *Osteoarthritis and Cartilage*, *25*(2), 309–320.

Zhu, G., Mallery, S. R., & Schwendeman, S. P. (2000). Stabilization of proteins encapsulated in injectable poly (lactide-co-glycolide). *Nature Biotechnology*, *18*(1), 52–57.

SUPPORTING INFORMATION

Additional supporting information may be found online in the Supporting Information section at the end of this article.

How to cite this article: Fathi-Achachelouei M, Keskin D, Bat E, Vrana NE, Tezcaner A. Dual growth factor delivery using PLGA nanoparticles in silk fibroin/PEGDMA hydrogels for articular cartilage tissue engineering. *J Biomed Mater Res*. 2019;1–22. https://doi.org/10.1002/jbm.b.34544